

## UvA-DARE (Digital Academic Repository)

### Cooperative Role of Water Molecules during the Initial Stage of Water-Induced Zeolite Dealumination

Stanciakova, K.; Ensing, B.; Göttl, F.; Bulo, R.E.; Weckhuysen, B.M.

**DOI**

[10.1021/acscatal.9b00307](https://doi.org/10.1021/acscatal.9b00307)

**Publication date**

2019

**Document Version**

Final published version

**Published in**

ACS Catalysis

**License**

CC BY-NC-ND

[Link to publication](#)

**Citation for published version (APA):**

Stanciakova, K., Ensing, B., Göttl, F., Bulo, R. E., & Weckhuysen, B. M. (2019). Cooperative Role of Water Molecules during the Initial Stage of Water-Induced Zeolite Dealumination. *ACS Catalysis*, 9(6), 5119-5135. <https://doi.org/10.1021/acscatal.9b00307>

**General rights**

It is not permitted to download or to forward/distribute the text or part of it without the consent of the author(s) and/or copyright holder(s), other than for strictly personal, individual use, unless the work is under an open content license (like Creative Commons).

**Disclaimer/Complaints regulations**

If you believe that digital publication of certain material infringes any of your rights or (privacy) interests, please let the Library know, stating your reasons. In case of a legitimate complaint, the Library will make the material inaccessible and/or remove it from the website. Please Ask the Library: <https://uba.uva.nl/en/contact>, or a letter to: Library of the University of Amsterdam, Secretariat, Singel 425, 1012 WP Amsterdam, The Netherlands. You will be contacted as soon as possible.

*UvA-DARE is a service provided by the library of the University of Amsterdam (<https://dare.uva.nl>)*

# Cooperative Role of Water Molecules during the Initial Stage of Water-Induced Zeolite Dealumination

Katarina Stanciakova,<sup>†</sup> Bernd Ensing,<sup>‡</sup> Florian Göttl,<sup>§</sup> Rosa E. Bulo,<sup>\*,†,⊥</sup> and Bert M. Weckhuysen<sup>\*,†,⊥</sup>

<sup>†</sup>Inorganic Chemistry and Catalysis Group, Debye Institute for Nanomaterials Science, Utrecht University, Universiteitsweg 99, 3584 CG Utrecht, The Netherlands

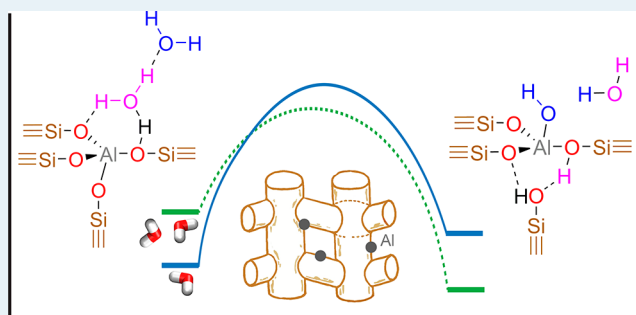
<sup>‡</sup>Van't Hoff Institute for Molecular Sciences, University of Amsterdam, Nieuwe Achtergracht 166, 1018 WV Amsterdam, The Netherlands

<sup>§</sup>Department of Chemical and Biological Engineering, University of Wisconsin–Madison, 1415 Engineering Drive, Madison, Wisconsin 53706, United States

## Supporting Information

**ABSTRACT:** Understanding water-induced zeolite dealumination is crucial for control of the hydrothermal stability of zeolite-based catalyst materials. Here we explore the dealumination process, focusing on the first Al–O(H) bond-breaking step in a density functional theory model of a ZSM-5 crystal in the presence of a single and two water molecules per active site. We identify a set of four possible reaction mechanisms consisting of two different types of reactions. In the first three proposed mechanisms, Al–O(H) bond breaking is induced by adsorption and dissociation of an incoming water molecule. The fourth mechanism is different and leads to a different reaction product, suggesting an alternative follow-up mechanism. In this energetically very favorable case, the breaking of the Al–O(H) bond is induced by nondissociative adsorption of two water molecules. We therefore assume that the proposed mechanism is a viable first dealumination step. This implies that all Al–O(H) bond-breaking mechanisms are initiated from metastable water adsorption modes, and water reorganization from the most stable mode needs to occur prior to hydrolysis of the Al–O(H) bond. We suggest that the feasibility of this rearrangement (Al accessibility) is one of the determining factors for the relative occurrence of dealumination at different sites. We further establish a correlation between the Al site susceptibility toward dealumination and reaction conditions, which can be further used during postsynthetic treatment of the zeolite to control Al distribution and thus hydrothermal stability of the catalyst.

**KEYWORDS:** zeolite, dealumination, water, ZSM-5, DFT, regioselectivity, Al distribution



## 1. INTRODUCTION

Zeolites have widespread applications in many areas, such as the petrochemical and chemical industry, gas adsorption and separation, and environmental protection.<sup>1,2</sup> The enormous industrial success of these crystalline aluminosilicate materials can be related to their activity, stability, and shape selectivity as solid catalysts in a wide range of chemical reactions. They are widely used in high-temperature oil refining processes, such as fluid catalytic cracking (FCC), hydrocracking, and aromatization.<sup>3,4</sup> The dwindling availability of fossil resources, combined with increasing atmospheric levels of CO<sub>2</sub>, creates a demand for further exploration of the zeolite applicability in industrial catalysis. One of the most pressing priorities is the development of chemical processes for the production of chemicals and fuels from alternative resources, such as biomass and municipal waste. These can be converted into valuable compounds like methanol and then used to produce hydrocarbons in the so-called methanol-to-hydrocarbons

(MTH) or methanol-to-gasoline (MTG) processes.<sup>5,6</sup> The development of new and efficient catalytic routes that can compete with traditional fossil-based conversion approaches via zeolite-based catalysis is a compelling course of action.<sup>7,8</sup>

Differences between the fossil feedstocks and renewable alternatives, such as biomass or municipal waste, present the main challenge in the development of the new processes. Biomass compounds are more oxygen-rich and hydrophilic in nature, which imposes new demands on the properties of the catalysts used to convert them. In biomass-based processes, the catalyst is exposed to water during all stages of its lifetime. At elevated temperatures, the water can hydrolytically remove aluminum atoms from the zeolite framework (dealumination), forming extra-framework aluminum species (EFALs), which

Received: January 22, 2019

Revised: April 13, 2019

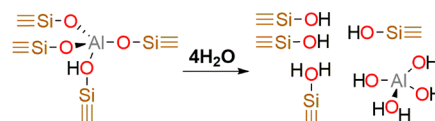
Published: May 3, 2019

leads to the partial or complete loss of Brønsted acid sites and the formation of mesopores. Introduction of mesopores is relevant for many industrial processes such as FCC as it ensures the optimal accessibility of acid sites and prevents the diffusion limitations of reactants and products.<sup>3,9</sup> Therefore, water-induced zeolite dealumination is traditionally harnessed during catalyst preparation for postsynthetic tailoring of the catalytic properties and maintenance of stability.<sup>9–12</sup> As has been recently shown, controlled dealumination has a great potential in the design of the hydrothermally stable and active catalyst for the biomass conversion as well.<sup>13,14</sup> During biomass conversion, water is often an abundant reaction byproduct or is cofed to control product yields and attenuate catalyst deactivation due to coking.<sup>15–19</sup> During catalyst regeneration (an essential part of the catalytic cycle that counters zeolite deactivation due to coking), steam is often still present, and it has been observed that on balance it exacerbates catalyst deactivation.<sup>17,20–22</sup>

The above examples demonstrate the clear importance of control over dealumination, as it is a key factor in the improvement of the stability and efficiency of the zeolite catalysts for current and future processes to produce chemicals. Surprisingly, knowledge about the reaction mechanism on the atomic scale is still rather limited. The most common experimental techniques, like <sup>27</sup>Al NMR or FT-IR spectroscopy, rely on bulk characterization of the zeolite ZSM-5 material, and analysis on a single atom level remains a difficult task. Nonetheless, some conclusions have been drawn. Ong et al.<sup>23</sup> extensively studied the dealumination of zeolite ZSM-5 with high Si/Al ratio. Using Co<sup>2+</sup> ion exchange, they found that two Al atoms in close vicinity show extraordinary hydrothermal stability compared with isolated Al atoms. Karwacki et al. used the combination of focused ion beam (FIB) and scanning electron microscopy (SEM) tomography to characterize steam-induced mesopore formation within zeolite ZSM-5 crystals. The observed nonuniform distribution of mesopores along various sections in steam-treated zeolite ZSM-5 led to the conclusion that the sinusoidal pores are more susceptible toward dealumination than the straight pores.<sup>24</sup> Holzinger et al.<sup>25</sup> investigated Al distribution using <sup>27</sup>Al MQMAS NMR spectroscopy before and after steaming of zeolite ZSM-5 and found out that Al sites in the intersection are the most prone toward dealumination. The only technique that can spatially resolve a distribution of individual atoms is the atomic probe tomography (APT). Perea et al. successfully applied APT on ZSM-5 crystals with the aim to investigate the aluminum distribution before and after steaming. It was found that steaming causes Al redistribution inside the zeolite crystal and leads to further clustering of Al atoms.<sup>26</sup> In the past few years, computational simulations have proven to be an essential tool to understand the interactions between water and zeolite on an atomic level. Using the semiempirical method CATIVIC,<sup>27</sup> Lisboa and co-workers<sup>28</sup> studied the formation of EFALs in the zeolite ZSM-5. Several reaction intermediates were found to be stable, penta-coordinated species with one to four covalent Al–O–Si bonds to the framework and hexa-coordinated species with two framework bonds. However, activation and reaction energies were not reported, and the feasibility of the proposed pathways still needs to be confirmed. Malola et al.<sup>29</sup> reported the first density functional theory (DFT) study of the dealumination process in which each step of the proposed five-step reaction mechanism is initiated by the adsorption of a single water molecule on the Brønsted acid site (BAS).

Formation of the various intermediates required very high activation energies (>190 kJ/mol). The final reaction product is the free Al(OH)<sub>3</sub>H<sub>2</sub>O EFAL compound and a defect (a silanol nest) in the zeolite framework (Scheme 1).

### Scheme 1. Proposed Dealumination Mechanism<sup>a</sup>

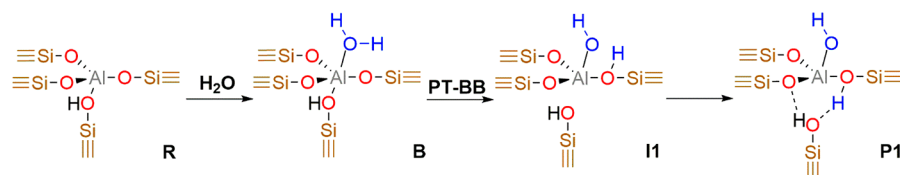


<sup>a</sup>See ref 29. The attack of four water molecules leads to the formation of Al(OH)<sub>3</sub>H<sub>2</sub>O EFAL species and a silanol nest.

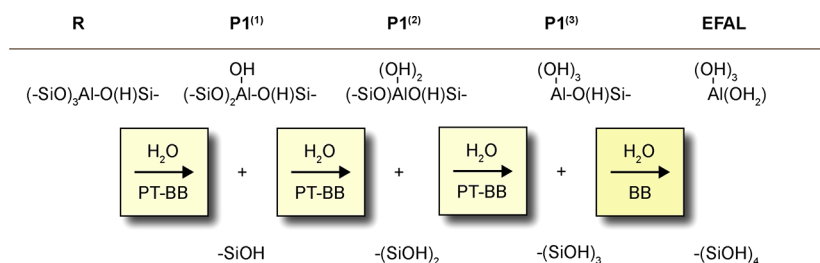
A more plausible mechanism for the first step of the process in Scheme 1 was recently proposed by Silaghi et al.<sup>30</sup> In this mechanism (Mechanism I, Scheme 2), the initial interaction between a water molecule and the zeolite is a coordination of the water molecule to the Al atom in the *anti*-position to the BAS proton (B, Scheme 2). This is followed by water dissociation via proton transfer (PT) onto one of the adjacent framework oxygen atoms leading to a formation of a new reaction intermediate (II, Scheme 2). The reaction product has already an Al–O(H) bond broken (BB) but is very unstable. In the last step of the reaction, the system rearranges so that the new framework proton forms a hydrogen bond with the silanol group, resulting into a more thermodynamically favorable product (P1, Scheme 2).

Formation of a free EFAL species is then expected to occur via three more steps (Scheme 3). The second and third steps are very similar to the first, involving water adsorption, water dissociation via proton transfer to framework oxygen atom, and subsequent Al–O(H) bond breaking (PT–BB). The final step is different, in which a bond breaking (BB) is not preceded by dissociation of the water molecule. The authors suggest that once the first Al–O(H) bond is broken, the Al atom gains flexibility, and Al–O(H) bond dissociation with equatorial (instead of axial) substitution of Si–OH becomes feasible as well.<sup>31</sup> Mechanism I (Scheme 2) was found to be rather universal, as it was computationally confirmed in different zeolite framework topologies (CHA, MOR, FAU, and MFI) always with low activation energies (76–125 kJ/mol). Like the first DFT study,<sup>29</sup> the proposed mechanism assumes a series of subsequent hydration steps with never more than one water molecule present. This single-water approach has also been applied in the study of similar processes, such as desilication or acid-catalyzed dealumination.<sup>32–34</sup> However, up to now, the possibilities and limitations of this approach have not been assessed.

In this work, we increase the complexity by modeling the dealumination of zeolite ZSM-5 as a system with two water molecules per Al site. Like Silaghi et al.,<sup>30</sup> we focus on the study of the initial stage of dealumination and select three different active site locations. Our results show that the water–water interactions strongly alter the mechanism and landscape of dealumination reaction. We propose three additional mechanisms for the first Al–O(H) bond-breaking reaction next to the possible mechanism proposed by Silaghi and co-workers.<sup>30</sup> The most prevalent ones are induced by either water-mediated proton transfer or nondissociative water adsorption. Each of the four pathways is initiated from a different active water adsorption mode, whereas we identify an

Scheme 2. Schematic of the Proposed Reaction Mechanism (Mechanism I) of Dealumination<sup>a</sup>

<sup>a</sup>See ref 30. The reaction is initiated by the adsorption of water on the Al atom in the *anti*-position to BAS proton (B), followed by subsequent water dissociation by way of proton transfer accompanied by Al–O(H) bond breaking (PT-BB). The final product P1 is the stable intermediate with the one Al–O(H) bond broken and three hydroxyl groups.

Scheme 3. Schematic Representation of the Four-Step Dealumination Process<sup>a</sup>

<sup>a</sup>The first three steps follow a mechanism like Mechanism I: water adsorption, water dissociation followed by a proton transfer (PT), and Al–O(H) bond breaking (BB, Scheme 2). In the final step, Al–O(H) bond breaking is induced without proton transfer (BB), and a free EFAL species is formed.

unreactive protonated water dimer as the most stable reactant state. Our results suggest that the stability of an Al site is at least partly determined by the reorganization of water molecules from the unreactive mode to the reactive starting structures, and the Al accessibility and reaction conditions are the key factors that determine its reactivity.

## 2. METHODS

**2.1. Structure of the Zeolite.** As a model system, the zeolite ZSM-5 structure (Figure 1) with the primitive orthorhombic unit cell with 12 distinguishable framework T-sites (T = Si or Al) was chosen. Three different periodic zeolite models were considered: a single Si atom at the intersection of the sinusoidal and the straight channel (T3, Figure 1), in the sinusoidal channel (T10, Figure 1), or in the straight channel (T11, Figure 1) was replaced by an Al atom.<sup>35</sup> These sites were chosen to be consistent with those used by Silaghi et al.<sup>30</sup> The substitution of Si by Al introduces a negative charge, which we compensate with an added proton. There are four oxygen atoms bonded to the asymmetric Al atom, and each of these can serve as the proton acceptor. Water adsorption energies were computed for all 12 combinations of protonation site and Al position. We label 12 different molecular models (Figure 1) T<sub>n</sub>O<sub>m</sub>, with  $n \in \{3, 10, 11\}$ , and  $m \in \{1-4\}$  (e.g., T3O4).

**2.2. Computational Details.** All simulations were performed using the CP2K software.<sup>36</sup> The Gaussian Plane Wave method<sup>37</sup> was employed with a TZVP basis set, GTH pseudopotentials, and PBE functional.<sup>38</sup> The reliability of PBE functional to reproduce reaction profiles for dealumination reaction has been validated by Malola et al., who tested the performance of PBE functional against hybrid B3LYP functional. The authors found only small differences in the obtained reaction profiles.<sup>29</sup> Additionally, Fischer benchmarked the performance of nine GGA functionals with and without dispersion corrections on the structures of water in various zeolite frameworks that contained multiple water

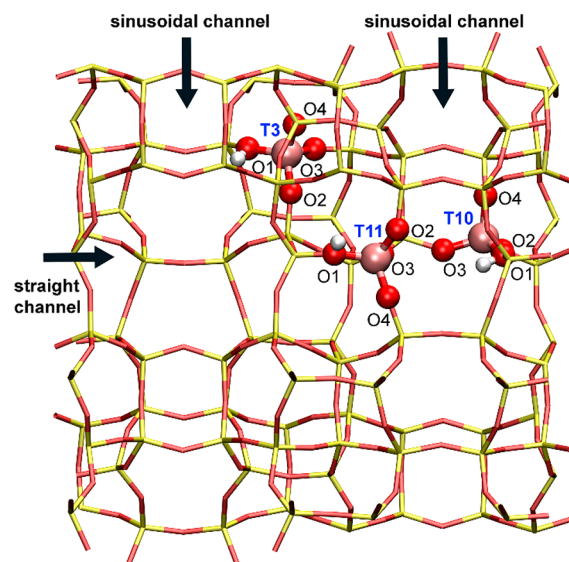


**Figure 1.** Zeolite H-ZSM-5 possesses the MFI topology. The orthorhombic unit contains 12 geometrically distinguished positions that can be occupied by an Al atom (T-sites), which provides in total 48 different possibilities for the position of a Brønsted acid site (BAS) proton. In our model was the Al atom (visualized by a pink ball) placed in the sinusoidal channel (T10), in the straight channel (T11) or at their intersection (T3).

molecules. The author found that PBE and PW91 functionals without dispersion corrections give the smallest overall deviation between experiment and computational results.<sup>39</sup> To further verify the performance of PBE functional and explore the effect of dispersion corrections, all adsorption energies and three reaction pathways were recomputed using PBE+D2 functional<sup>40</sup> (Supporting Information, Figure S1–S2, Table S1). The results show that there is very good agreement between the functionals, and the same trends are captured

when comparing different reaction mechanisms even with multiple water molecules present. The main difference between PBE and PBE-D2 approach is in the absolute values of adsorption energies; however, the trends are preserved also in that respect. This is in agreement with findings of Fjermestad et al., who showed that the dispersion corrections do not significantly alter the reaction profile; they only affect the adsorption energies.<sup>33</sup> Additionally, we have examined the influence of -D2 dispersion corrections on the free energy profiles as discussed in Section 3.6.2.

As the first step in the creation of the model system, the unit cell size of the pure Si structure (silicalite) was optimized. The initial stage of the optimization involved ab initio molecular dynamics simulations (AIMD) in the isothermal–isobaric ensemble (NPT). The time step for the integration of the equations of motion was 2 fs, and the system was equilibrated for 3 ps at 400 K and 1 bar. Subsequently, a simulation of 10 ps in canonical ensemble (NVT) was performed, using the equilibrated cell parameters ( $20.360 \times 20.156 \times 13.586 \text{ \AA}^3$ ). The structures of five distinct “snapshots” with the lowest potential energy were collected from the NVT simulation and optimized. From the resulting five geometries, the one with the lowest energy was used as the initial structure for all subsequent calculations. Because of very low Al concentration (Si/Al = 95), we assume that the introduction of Al induces only the negligible change in the unit cell parameters. Therefore, after the Al substitution, the unit cell parameters of the relaxed structure were kept fixed to their original values.

The adsorption energy  $E_{\text{ads}}$  for each Al and BAS proton positions ( $TnOm$  label) is reported with respect to the energy of the water-free zeolite with the most stable BAS proton position for a given Al site (T3O2, T10O1, and T11O4), with a correction for water adsorption from a physisorbed state (see below).<sup>41</sup> The geometries were considered as stable when their  $E_{\text{ads}} < 100 \text{ kJ/mol}$ ; otherwise, they were excluded from the further analysis, and the corresponding values are reported only in Supporting Information (Tables S2–S3).

Reaction pathways were explored using Nudged Elastic Band (NEB) with 10 or 20 images.<sup>42</sup> Transition states were localized using a transition state search via the Dimer Method<sup>43</sup> and confirmed using vibrational analysis. In some situations, the imaginary frequency was very low (less than  $200 \text{ cm}^{-1}$ ), which can be attributed to the very flat potential energy landscape of zeolites. In those cases, the validity of the state was supported by the match between the imaginary vibration and the reaction coordinate. Pathway activation energies  $E_a$  are defined as the energy difference between the highest transition state and the reactant structure of zeolite with adsorbed water molecules ( $E_{\text{max}}^\ddagger - E_{\text{reactant}}$ ). For all calculations, the target accuracy for the SCF convergence was set to  $10^{-7}$ , except vibrational analysis, where the value of  $10^{-8}$  was used. The convergence criteria for the optimization of stationary points were set to the default CP2K values except the maximum geometry change between the current and the last optimizer iteration that was set to  $0.00013 \text{ \AA}$ , and the criterion for the root-mean-square geometry change between the current and the last optimizer iteration that was set to  $0.00026 \text{ \AA}$ .

The Gibbs free energy profiles were calculated for the temperatures between 300 and 1000 K with step of 25 K and at pressure 1 bar using a full vibrational analysis within a harmonic approximation. The vibrational analysis was applied on all reaction intermediates, including transition states. To minimize the effect of spurious imaginary frequencies on the

free energy profiles, we followed the methodology from the literature,<sup>44,45</sup> where the low frequency vibrational modes are replaced by a wavenumber of a fixed value. In this case, a cutoff value of  $100 \text{ cm}^{-1}$  was used. For the analysis of vibrational frequencies, the software TAMKIN was used.<sup>46</sup> As a thermodynamic reference for water, the corrected physisorbed water state proposed by Nielsen et al.<sup>41</sup> has been considered:

$$G_{\text{H}_2\text{O}}(T) = H_{\text{H}_2\text{O,ideal}} + dH_{\text{ads}} - T(S_{\text{H}_2\text{O,ideal}}(T) - C)$$

where  $G_{\text{H}_2\text{O}}$  denotes the Gibbs free energy of the water molecule at given conditions,  $H_{\text{H}_2\text{O,ideal}}$  is enthalpy of a water molecule modeled as an ideal gas,  $dH_{\text{ads}}$  corresponds to the experimental asymptotic limit of adsorption enthalpy of water in HZSM-5 ( $-42 \text{ kJ/mol}^{-1}$ )<sup>47</sup> and  $C$  is the gas-phase entropy constant ( $114 \text{ J mol}^{-1} \text{ K}^{-1}$ ).<sup>41</sup>

Finally, we use the calculated free energies to compare the preferences of reaction pathways and the reactivity of Al sites under realistic conditions. We assume that the prefactors in all reactions are comparable and the different adsorption modes at each Al site are equilibrated. For each of the Al sites, we therefore calculate the temperature-dependent Gibbs free energy of the highest transition state as

$$G_{Tn,M+x\text{H}_2\text{O}}^{\ddagger,\text{max}}(T, p) = G_{Tn,M+x\text{H}_2\text{O}}^{\ddagger,\text{max}}(T) - x \left( G_{\text{H}_2\text{O}}(T) + \ln \frac{p_{\text{H}_2\text{O}}}{p_0} \right) - G_{Tn}(T)$$

where  $Tn$  stands for the different Al sites,  $G(T)$  are the entropy corrected DFT energies,  $G^{\ddagger,\text{max}}(T)$  is the highest energy along the reaction pathway of mechanism  $M$ ,  $x$  is number of water molecules in the system and the water pressure  $p_{\text{H}_2\text{O}}$  is included as pressure correction with respect to a reference pressure  $p_0$  at 1 bar. To explore the effect of dispersion interactions, we modeled the reaction profiles for both PBE and PBE-D2 functional using the assumption that the introduction of -D2 correction affects only the adsorption energies but does not affect the shape of the reaction profiles. In the case of PBE-D2, van der Waals interactions are included by correcting all PBE energies of the initial stable adsorbates by the -D2 correction. The free energies of the reaction intermediates and transition states of the Al–O(H) bond breaking were shifted for each reaction separately, by the size of -D2 correction of the corresponding initial stable adsorbate. The transition states in water reorganization were corrected by the average -D2 correction of the initial and final adsorption mode.

### 3. RESULTS AND DISCUSSION

This section is organized as follows: in Section 3.1, we first describe possible adsorption modes of the single and two water molecules in the zeolite framework, and in Section 3.2, we discuss the impact of an additional water molecule on the overall dealumination scheme. Section 3.3 describes four different mechanisms for breaking of the Al–O(H) bond, the first of which is the mechanism depicted in Scheme 2 of the Introduction.<sup>30</sup> In Section 3.4, we present a mechanism for water rearrangement among the different adsorption modes, and in Section 3.5, we discuss the effect of water rearrangement on the relative energetics of the Al–O(H) bond-breaking reactions. Finally, in Section 3.6, the influence of reaction conditions on dealumination is assessed.

### 3.1. Water Adsorption to the Zeolite Framework.

With the aim to understand the impact of multiple water molecules on the mechanism of dealumination, we first investigate the preferred location of these water molecules in the zeolite ZSM-5. We discuss the adsorption of a single water molecule to the zeolite framework and then the effect of a second water molecule on the adsorption energetics. We do this for three different Al positions in the framework (T3, T10, and T11) with all possible combinations of BAS position (O1–O4).

**3.1.1. Adsorption of a Single Water Molecule.** In agreement with the observations of Silaghi et al.,<sup>30</sup> the adsorption of one water molecule in a protonated zeolite ZSM-5 (HZSM-5) is a competition between a coordination to the BAS proton (A, Figure 2), and a coordination to the Al

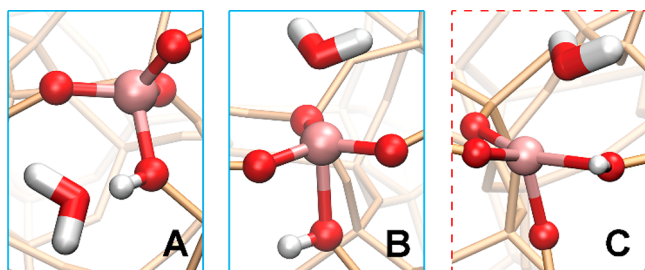


**Figure 2.** First water molecule can coordinate either to the BAS (A) or to the Al atom in the *anti*-position to the BAS (B), which results in the Al–O(H) bond elongation. Also, the adsorption on the Al in *syn*-position is possible (C), but in general not favored.

atom in the *anti*-position to the BAS (B, Figure 2). Mode B plays a role in the mechanism proposed by Silaghi et al. (Scheme 2).<sup>30</sup> A third coordination mode with the water molecule to the Al atom in *syn*-position to the BAS proton (C, Figure 2) is not energetically stable for most of the  $T_nO_m$  models and will not be discussed in more detail. Complexes A and B are both stabilized by one or two additional hydrogen bonds between the water molecule and the zeolite framework. In general, mode A is thermodynamically preferred over B with adsorption energies  $-24 \pm 9$  kJ/mol and  $3 \pm 21$  kJ/mol, respectively as shown in Table 1. After coordination to the Al atom (B and C), the water molecule acts as a Lewis base by donating a free electron pair to the Al atom, establishing a fifth Al–O bond. The newly formed bond is of the same length ( $2.05 \pm 0.03$  Å) as the Al–O(H) bond and leads to an elongation of that bond up to  $2.06 \pm 0.09$  Å. The destabilization of the Al–O(H) bond explains the weaker adsorption on the Al atom in mode B. The results agree closely with those obtained by Silaghi et al.,<sup>30</sup> provided that the adsorption energies for each of the 12  $T_nO_m$  models are expressed with respect to the energy of the equivalent empty framework (the same  $m$ -value instead of the most stable one), and a physisorbed water<sup>41</sup> is used as a reference structure. The

adsorption energies of both modes for each of  $T_nO_m$  sites are shown in Supporting Information (Figure S1, Table S2) where they are also compared to PBE-D2 adsorption energies.

**3.1.2. Adsorption of Two Water Molecules.** The adsorption of two water molecules is more complex. We distinguish four important stable configurations that can be divided into two groups on the basis of their activity. Three of the stable configurations (A', B', C', Figure 3) are *active adsorption intermediates* that can serve as starting geometries for the dealumination pathway. In contrast, the most stable configuration, an asymmetric Zundel ion  $H_5O_2^+$  (D', Figure 3) does not act as a direct precursor for the initial Al–O(H) bond-breaking reaction and can be considered a *nonactive adsorption mode*. The adsorption energies of all stable structures are shown in Figure 4 and are tabulated in Supporting Information (Table S3). The adsorption energies were also recomputed using PBE-D2 functional (see Supporting Information, Figure S2).

Active adsorption intermediate A' coordinates  $H_2O^{(1)}$  to the Al atom in the *anti*-position to the BAS proton and  $H_2O^{(2)}$  to the BAS proton (A', Figure 3). The stable geometries show an adsorption energy of  $-10 \pm 30$  kJ/mol. Interestingly, the adsorption energies are smaller than the sum of adsorption energies for single water modes A and B (except for the adsorption on T3O2); therefore, there must be a destabilizing competition between the adsorption of water on BAS proton (A) and on the Al atom (B). Indeed, the coordination of  $H_2O^{(1)}$  on the Al atom results in a weakening of the hydrogen bond between the BAS proton and  $H_2O^{(2)}$ , which is on average elongated by 0.1 Å compared with mode A. The Al–O(H) bond is 0.1 Å less elongated when compared with equivalent structures in mode B. The competition between water molecules to bind to the active site indicates that sufficient amounts of water needs to be present in the system before the mode A' is formed. It is therefore reasonable to expect that different amounts of water will be adsorbed on the active site at varying pressures and temperatures. Because the adsorption modes act as starting geometries of the Al–O(H) bond breaking, this suggests that reaction conditions impact the dealumination mechanism, which is discussed in next sections.

The most stable of all *active adsorption modes* is B', which coordinates both water molecules to the Al atom in the *anti*-position to the BAS proton, while only  $H_2O^{(1)}$  is directly coordinated (C', Figure 3). The  $H_2O^{(2)}$  molecule does not have any direct interaction with the Al atom, but it is stabilized by a strong hydrogen bond to  $H_2O^{(1)}$  ( $1.61 \pm 0.05$  Å). The Al–O(H) bond in C' is always elongated but falls into two separated ranges: a significant Al–O(H) bond elongation ( $2.06$ – $2.45$  Å) and a broken Al–O(H) bond ( $2.77$ – $3.12$  Å). The adsorption energies of the most stable structures are  $-33 \pm 25$  kJ/mol with average Al–O(H) bond length of  $2.47 \pm 0.39$  Å. Compared to the corresponding single water mode B,  $H_2O^{(2)}$  in B' induces not only further elongation of the Al–

**Table 1.** Adsorption Energies and Al–O(H) Bond Lengths of the Stable Adsorption Modes of a Single and Two Water Molecules to a HZSM5 Active Site

adsorption mode	$E_{\text{ads}}$ [kJ/mol]	Al–O(H) [Å]	adsorption mode	$E_{\text{ads}}$ [kJ/mol]	Al–O(H) [Å]
A	$-24 \pm 9$	$1.89 \pm 0.02$	A'	$-10 \pm 30$	$2.03 \pm 0.6$
B	$3 \pm 21$	$2.06 \pm 0.09$	B'	$-33 \pm 25$	$2.47 \pm 0.39$
C	-	-	C'	$21 \pm 26$	$1.93 \pm 0.03$
			D'	$-73 \pm 4$	-

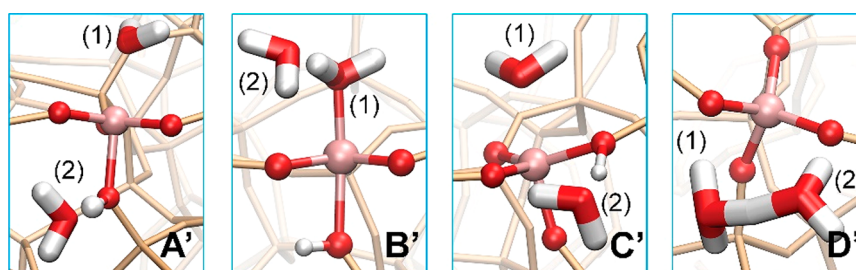


**Figure 3.** Visualization of four different adsorption modes via which the initial interaction of two water molecules with the zeolite occurs: two water molecules coordinate simultaneously to the BAS proton and to the Al atom in the *anti*-position to the BAS proton (A'); to the Al atom in the *anti*-position to the BAS proton with only one water molecule coordinated on the Al atom (B'); to the Al atom in the *syn*-position to the BAS proton and the BAS proton (C'); to the BAS proton to form an asymmetric Zundel ion,<sup>48</sup> which is the most stable configuration. The stability of each of the adsorption modes was tested for all positions of BAS around T3, T10, and T11 site.

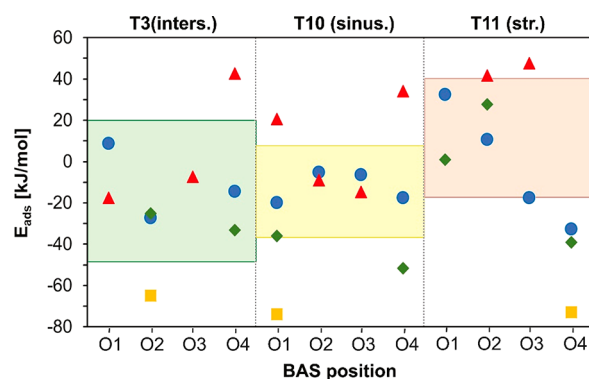


**Figure 4.** Adsorption energies of two water molecules on T3, T10, and T11 sites in combination with all possible BAS positions (O1–O4). The adsorption energies are computed with respect to the most stable BAS positions of a given Al site (T3O2, T10O1, and T11O4). Four adsorption modes are possible: the adsorption of two water molecules on the BAS proton and on the Al atom in the *anti*-position to the BAS proton (A', blue ●); on the Al atom in the *anti*-position to the BAS proton with only one water molecule coordinated on the Al atom (B', green ◆); on the Al atom in the *syn*-position to the BAS proton and the BAS proton (C', red ▲); and a formation of Zundel ion (D', yellow ■). To visually capture differences in accessibility between Al sites, colored rectangles centered on the median  $E_{\text{ads}}$  with the area indicating standard deviation are shown.

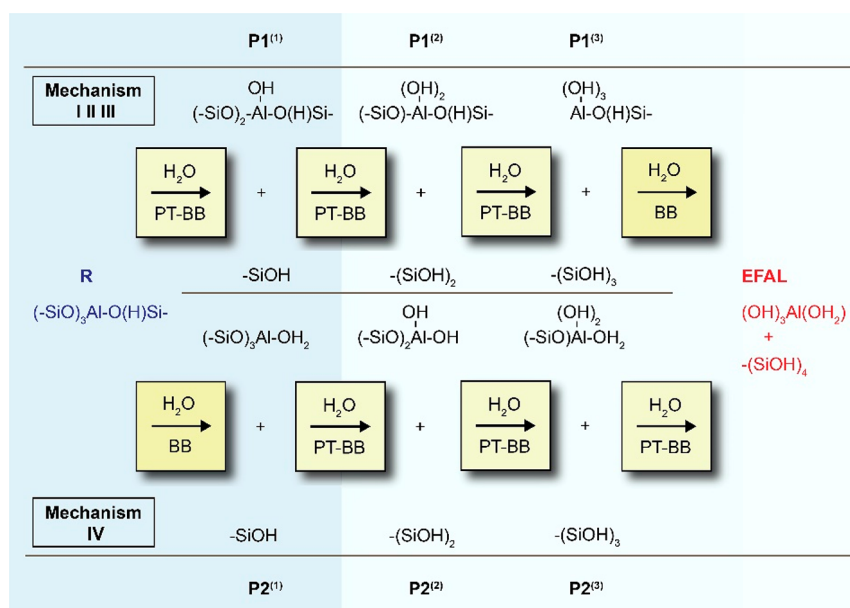
O(H) bond but also shortening of the Al–OH<sub>2</sub><sup>(1)</sup> distance by up to 0.15 Å (T10O4 and T3O4). This can be explained by increased electron donation from the combined water molecules to the Al atom, further promoting the breaking of the Al–O(H) bond.

Very similar to adsorption mode A' is adsorption mode C', which coordinates H<sub>2</sub>O<sup>(1)</sup> to the Al atom in the *syn*-position (non-*anti*) to the BAS proton and H<sub>2</sub>O<sup>(2)</sup> to the BAS proton (C', Figure 3), with adsorption energies of  $21 \pm 26$  kJ/mol. It is worth noting that, in contrast to mode A', the stability of mode C' strongly depends on the framework model (TnOm). For some combinations (e.g., T11O1 or T11O4), steric constraints preclude formation of a stable structure. When the *anti*-position to the BAS proton is not accessible, C' represents a stable alternative to A' and vice versa. With only one water molecule present, an adsorption on the Al atom in the *syn*-position (C) is generally not stable. H<sub>2</sub>O<sup>(2)</sup> adsorbed on BAS proton makes the adsorption in *syn*-position possible. The distinctive feature of mode C' is that there is no significant elongation of the Al–O(H) bond (Table 1).

The asymmetric Zundel ion (D') is the most stable of all modes explored, with adsorption energies  $-73 \pm 4$  kJ/mol. The formation of such Zundel ions has been demonstrated in other works, computationally<sup>49</sup> as well as experimentally, especially using IR spectroscopy.<sup>50,51</sup> The H<sub>3</sub>O<sup>+</sup>–H<sub>2</sub>O complex is bound to the zeolite framework with two to four hydrogen bonds and has an H<sub>2</sub>O<sup>(1)</sup>–H bond of  $1.04 \pm 0.01$  Å and H<sub>2</sub>O<sup>(2)</sup>–H of  $1.53 \pm 0.04$  Å. This is different from the findings of Jungsuttiwong et al.,<sup>48</sup> who identified an asymmetric Zundel ion as the stable equilibrium structure of a water dimer in HZSM-5. While mode D' is the lowest energy structure, we find that dealumination cannot be initialized from this state directly.

Preliminary conclusions can now be drawn regarding the hydrothermal stability of the Al sites. The active adsorption modes at T3 and T10 sites are distributed around a median adsorption energy of  $-14 \pm 34$  kJ/mol and  $-13 \pm 22$  kJ/mol, respectively. The stable adsorbed species at T11 site have a median adsorption energy of  $11 \pm 29$  kJ/mol. The subtle difference can be explained by differences in the local framework structure, which result in more steric hindrance at T11 site. If the reaction intermediates are indeed precursors for dealumination, then the lower stability suggests superior hydrothermal resistance of Al located in the straight channel when the adsorption of two water molecules is preferred. These findings are in line with experimental observation of Karwacki et al.<sup>24</sup> and Holzinger et al.,<sup>25</sup> who independently assigned the highest hydrothermal stability to Al atoms located in the straight channel.

**3.2. Some Reflections on the Al–O Bond-Breaking Reaction.** By exploring the effect of water–water interactions on the Al–O(H) bond breaking reaction we identify four different reaction mechanisms (I, II, III, and IV). The first three mechanisms pursue the route outlined in the introduction (water dissociation followed by Al–O(H) bond breaking, Scheme 3), while in Mechanism IV, the Al–O(H) bond breaking is induced solely by water coordination resulting in a formation of a new reaction product P2 bonded to three framework oxygen atoms and a water molecule. The four steps to a formation of a free EFAL species need to follow (1: BB) – (2: PT-BB) – (3: PT-BB) – (4: PT-BB) instead of (1: PT-BB) – (2: PT-BB) – (3: PT-BB) – (4: BB), where PT and BB stand for proton transfer and Al–O(H) bond breaking, respectively. The latter mechanism would initiate an alternative route to the EFAL product, as depicted in Scheme 4, which may have consequences on the shape of the reaction profile of the whole dealumination reaction. In Mechanisms I–III the

Scheme 4. Schematic Representation of the Four-Step Dealumination Process Starting from Mechanism I, II, or III (Top), and from Mechanism IV (Bottom)<sup>a</sup>

<sup>a</sup>In both cases, in total three proton transfer reactions followed by Al–O(H) bond breaking (PT-BB) and one only Al–O(H) bond-breaking reaction (BB) are required for the formation of the Al(OH)<sub>3</sub>H<sub>2</sub>O EFAL product. In this work, we focus only on the initial stage of the reaction (depicted in blue).

first three reaction steps are the most energetically demanding, while the last step of the reaction only requires the adsorption of water molecules followed by Al–O(H) bond breaking. In Mechanism IV, the order of these steps is reversed, therefore the viability of this reaction route has to be further confirmed by modeling of the whole reaction pathway. We identify this as a topic for further study and here we only propose a possible scheme of the whole dealumination pathway (shown in Scheme 4). In the following, we discuss these four mechanisms in more detail.

**3.3. Breaking of the Al–O(H) Bond.** **3.3.1. Mechanism I: H<sub>2</sub>O<sup>(2)</sup> as Spectator.** Mechanism I is the mechanism proposed by Silaghi et al.,<sup>30</sup> which follows the PT-BB route. Since the reaction requires a water molecule coordinated to the Al atom in the *anti*-position to the BAS proton, only adsorption modes B, A', and B' can be considered as possible starting configurations. Out of the 12 TnOm models, we selected for each *n*-value the model with the most energetically favorable adsorption of one water molecule in mode B (T3O4, T10O1, and T11O4, see Supporting Information, Figure S1).

**Reactant A: 1 H<sub>2</sub>O.** As a first step, we calculate the energetics of the mechanism in Scheme 2 in the presence of one water molecule. We find that the reaction in the T3O4 model (intersection) has an activation energy of  $E_a = 86$  kJ/mol, while the same reaction in the T10O1 (sinusoidal) and T11O4 (straight) models have a significantly higher energy barrier ( $E_a = 103$  kJ/mol). This is in qualitative agreement with the results obtained by Silaghi et al.<sup>30</sup> and suggests that the T3O4 site is most likely to break a first Al–O(H) bond. However, in our work lower barriers (Table 2) ( $\Delta E_a = 17$  kJ/mol for T10O1) are found, which we expect is caused by differences in the BAS proton positions, the functional (PBE vs PBE-D2) and software used (CP2K vs VASP). The corresponding reaction profiles together with structural information on all stationary points along the reaction pathway

**Table 2. Adsorption Energies  $E_{ads}$ , Relative Stabilities of the Reaction Intermediate II, Activation Energies  $E_a$  and Reaction Energies  $\Delta E$  (in kJ/mol) for the First Al–O(H) Bond-Breaking Reaction According to Mechanism I<sup>a</sup>**

Al location	adsorption mode	$E_{ads}$	$\Delta I1$	$\Delta E$	$E_a$
T3O4 (inters.)	B	3	75	43 (26)	86 (86)
	A'	−14	57	52	104
	B'	−18	-	63	102
T10O1 (sinus.)	B	−14	79	54 (83)	103 (120)
	A'	−20	39	67	102
	B'	−36	-	74	126
T11O4 (str.)	B	−18	86	53 (79)	103 (101)
	A'	−33	-	62	127
	B'	−34	-	69	120

<sup>a</sup>The literature values of the single water model<sup>30</sup> are listed in parentheses.

are shown in Supporting Information (Figures S3–S4, Tables S4–S7).

**Reactant A': 2 H<sub>2</sub>O.** Adsorption mode A' displays an elongated Al–O(H) bond, but the elongation is less than in mode B (Table 1). As a result, a higher activation energy for the Al–O(H) bond-breaking process may be expected. Indeed, we observe an increase in activation energy of 18 and 24 kJ/mol for the T3O4 and the T11O4 models, respectively. For the T10O1 model, no significant barrier change was observed upon introduction of H<sub>2</sub>O<sup>(2)</sup> (Table 2). Moreover, coordination of H<sub>2</sub>O<sup>(2)</sup> to the BAS proton reduces the stability  $\Delta E$  of reaction product P1 by prohibiting formation of a hydrogen bond between the newly formed silanol entity and the framework (Figure 5) about  $\Delta\Delta E = 9$ –13 kJ/mol for all Al sites as shown in Table 2.

Nonetheless, H<sub>2</sub>O<sup>(2)</sup> actively participates in the reaction and assists in the rotation of the proton. A new reaction



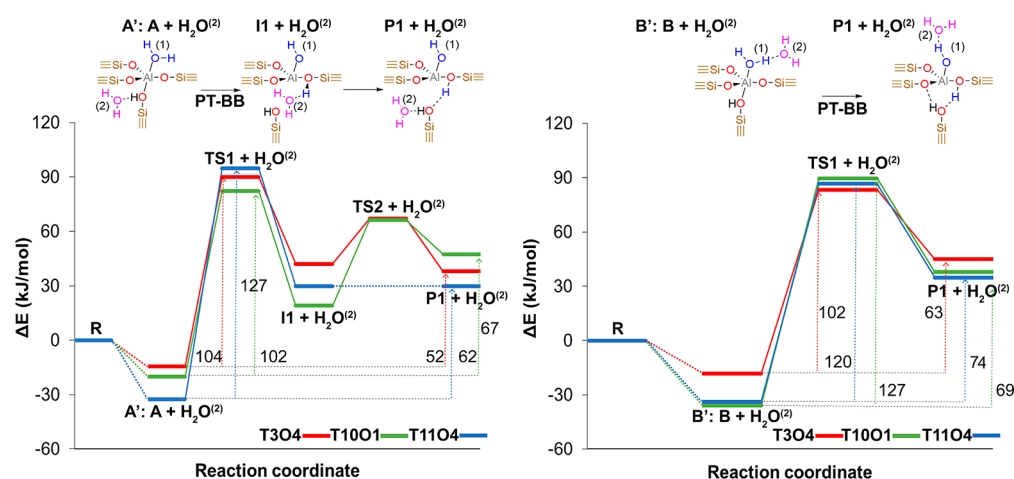


**Figure 5.** Reaction profiles of Mechanism I for two water molecules model. Two starting configurations were considered: the adsorption of water molecules in mode A' (left) or B' (right). The adsorption of second water molecule to the BAS proton (A') prevents formation of a hydrogen bond between Si–OH group and the framework oxygen that stabilizes the product P1 (Scheme 2). Instead, the additional hydrogen bond is formed between Si–OH and water (P1, left). R represents the empty zeolite, and its energy is corrected for two physisorbed water molecules. PT and BB (below arrows in the schemes) refer to proton transfer and Al–O(H) bond-breaking steps.

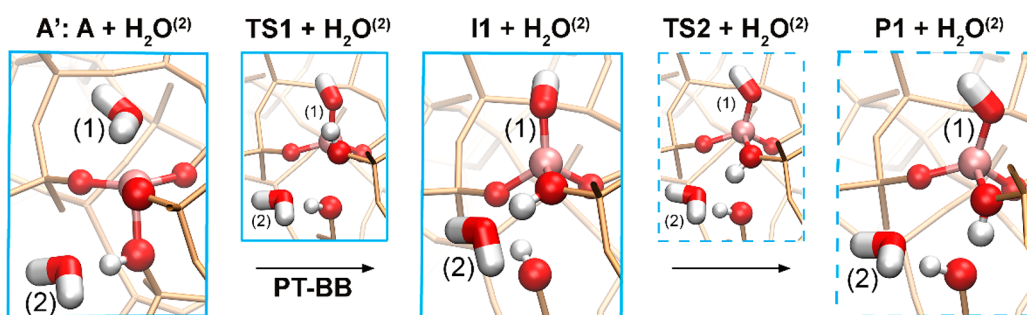


**Figure 6.** Mechanism I for the initial Al–O(H) bond-breaking reaction in the presence of two water molecules for T3O4 starting from the active adsorption mode A'. During the reaction, an additional water molecule  $\text{H}_2\text{O}^{(2)}$  moves away from the BAS proton and forms a hydrogen bond with the newly protonated oxygen atom, leading to a formation of very stable intermediate  $\text{I1} + \text{H}_2\text{O}^{(2)}$ . Therefore, the last reaction step from the single water molecule model (Scheme 2), a proton rotation, is not necessary anymore.

intermediate derived from a single water molecule model (I1, Scheme 2) is found, in which the coordinated water molecule  $\text{H}_2\text{O}^{(2)}$  moves away from the original BAS proton and forms a hydrogen bond with the newly protonated oxygen atom (Figure 6). For the T1001 active site, the new reaction intermediate is even more stable ( $\Delta\Delta E = -28$  kJ/mol) than the original reaction product P1 ( $\Delta E = 67$  kJ/mol). As a result, the last step of the reaction, a proton rotation, is not necessary anymore. The formation of the very stable intermediate  $\text{I1} + \text{H}_2\text{O}^{(2)}$  was not observed for the T1104 model, because in this case the BAS proton points toward a neighboring channel and the newly protonated oxygen atom is not accessible to it.  $\text{H}_2\text{O}^{(2)}$  cannot actively participate in the reaction, and therefore, the increase in activation barrier with respect to the one water molecule is large ( $\Delta E_a = 24$  kJ/mol). We can conclude that the coordination of a second water to the BAS proton alters the reaction profile and slows down the reaction thermodynamically (T3O4, T1001, T1104) or kinetically (T3O4, T1104).

**Reactant B': 2  $\text{H}_2\text{O}$ .** Contrary to the B mode, adsorption mode B' results in further activation of Al–O(H) bond with respect to the adsorption of a single water molecule in mode B, and thus, lower activation energies for bond breaking may be expected. However, we find that the activation energy increases with  $\Delta E_a = 16$ – $24$  kJ/mol for all modeled reaction pathways

(Table 2). Due to the coordination of  $\text{H}_2\text{O}^{(2)}$ ,  $\text{H}_2\text{O}^{(1)}$  is more electron rich, which makes water dissociation more energetically demanding. To quantify the electron enrichment of  $\text{H}_2\text{O}^{(1)}$  Hirschfeld charges were recomputed on a simple system of two water molecules in the configuration identical to their configuration in adsorption mode B'. We did this for all  $\text{TnOm}$  sites, where adsorption mode B' is stable. We observe the change of the total charge on  $\text{H}_2\text{O}^{(1)}$  by  $-0.06 \pm 0.03$  au compared to a single water molecule. Computed Hirschfeld charges are tabulated in Supporting Information (Table S8). The consequences on the evolution of energy barriers after electron enrichment of  $\text{H}_2\text{O}^{(1)}$  were further explored by computing proton affinities (PA) of  $\text{OH}^-$  residue in a single water molecule and a water dimer in three different configurations of mode B' (T3O4, T1001, T1104) as starting points. The results are summarized in Supporting Information (Table S9) PA for a single water molecule is 1471 kJ/mol, while for two water molecules, it is  $1558 \pm 1$  kJ/mol, indicating that the proton is bound more strongly to the water molecule when being part of B'. Therefore, the higher energy barrier for its dissociation might be expected.

Overall, the  $\text{H}_2\text{O}^{(2)}$  molecule does not actively participate in the reaction; structurally, the reaction intermediates are largely unaffected by  $\text{H}_2\text{O}^{(2)}$ , but they are less stable by 16–20 kJ/mol (Table 2). Therefore, the reaction is thermodynamically less

favorable, which we relate to the extraordinary stability of adsorption mode B'.

**Summary Mechanism I.** Our results show that when compared to the single molecule model, the presence of multiple water molecules alters the relative reaction probability of Al sites toward the first Al–O(H) bond breaking (Table 2). In the presence of a single-water molecule (mode A), the first Al–O(H) bond is less likely to break in the T10O1 and T11O4 model ( $E_a = 103$  kJ/mol) than in the T3O4 model ( $E_a = 86$  kJ/mol). Contrary, using two water molecules removes the difference between T3O4 and T10O1 ( $E_a = 102$  kJ/mol), but the reaction in the T11O4 model becomes the least likely with  $E_a = 120$  kJ/mol as shown in Figure 5. In general, the introduction of a second water molecule increases barriers with up to 24 kJ/mol (A', T11O4) and impairs the thermodynamic stability of the product P1. This confirms the necessity to include multiple water molecules, when modeling the reaction kinetics at conditions corresponding to higher water loadings. All energies and structural data of Mechanism I for both water models are summarized in the Supporting Information (Figure S4, Tables S4–S7).

**3.3.2. Mechanism II: Water-Mediated Proton Transfer.** It stands to reason that an alternative to the direct proton transfer reaction in Mechanism I is a proton transfer along a chain of water molecules (Figure 7). We label this Mechanism II, which can only have dually coordinated mode B' as its starting structure.

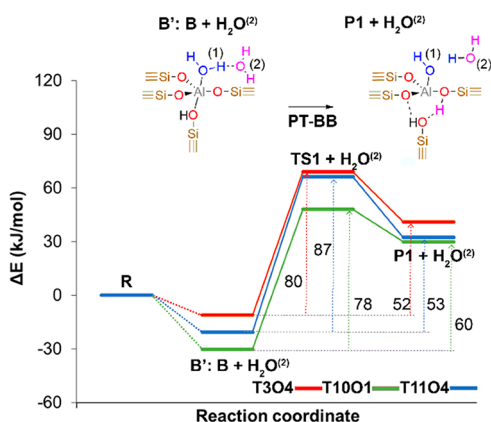


**Figure 7.** Mechanism II: A concerted proton transfer Al–O(H) bond-breaking mechanism (PT-BB), in which the proton transfer occurs along a chain of the two water molecules,  $\text{H}_2\text{O}^{(1)}$  and  $\text{H}_2\text{O}^{(2)}$ . Profiles are presented for three selected models with different Al positions: T3O4 (intersection), T10O1 (sinusoidal), and T11O4 (straight). R represents the empty zeolite, and its energy is corrected for two physisorbed water molecules.

**Reactant B': 2  $\text{H}_2\text{O}$ .** While Mechanism I can be seen as a stepwise process, we find that Mechanism II is a concerted process. In Mechanism I, the reaction product P1 is only stable once the system has reorganized after water dissociation to allow H-bond formation between the new proton and the O(H) leaving group. In Mechanism II, the flexibility of the water chain allows the proton to be deposited directly in the optimal position. In the reaction product, the remaining water molecule  $\text{H}_2\text{O}^{(2)}$  can either coordinate to the Al atom in P1 (T3O4), to the newly formed BAS proton of P1 (T10O1), or to the hydroxyl group of P1 (T11O4). The exact structure and stability of the product depends on the Al site position and the

local zeolite framework. The activation energies for all three models range from 78 to 87 kJ/mol (Figure 7), which is lower than the activation energies in Mechanism I. The narrow range of the activation energies, as well as the reaction energies ( $\Delta E = 52$ –60 kJ/mol), suggests that contrary to Mechanism I no particularly reactive Al site can be identified. All energies and structural data of Mechanism II are summarized in the Supporting Information (Tables S10–S11, Figure S5).

**Summary Mechanism II.** The low activation energies clearly demonstrate that the active participation of multiple water molecules can significantly accelerate the reaction and reduce the differences in reaction probabilities compared with the Mechanism I. The combined results suggest that the reactivity of an Al site might be determined by other factors, such as the accessibility of the Al atom dictated by local steric constraints, or the stability of the Al atom in the zeolite framework itself.

**3.3.3. Mechanism III: Water Insertion.** Both Mechanisms I and II require coordination of at least one water molecule to the Al atom in the *anti*-position to the BAS proton. As shown in Section 3.1.2, the stability of a given adsorption mode depends on the local framework, and due to the steric constraints, the *anti*-position to the BAS is not always accessible to water (e.g., T3O1, Figure 4). In this situation, an alternative mechanism is more viable: Mechanism III, starting solely from the adsorption mode C (1  $\text{H}_2\text{O}$ ) or C' (2  $\text{H}_2\text{O}$ ). Mechanism III is a consecutive reaction pathway that belongs to the PT-BB family but follows a more complex route.

**Reactant C: 1  $\text{H}_2\text{O}$ .** The reaction starts by adsorption of a water molecule in mode A followed by rearrangement into mode C (Figure 8, left). The water molecule (coordinated to the Al atom) is then incorporated into the zeolite framework forming a vicinal disilanol structure, while a proton is transferred to neighboring framework oxygen (I2, Figure 8, left). In the next step, the Al–O(H) bond is subsequently broken, while an O–Si bond in the vicinal disilanol structure also breaks and the product P1 is formed. The existence of a vicinal disilanol defect was proposed before,<sup>52,53</sup> together with a corresponding dealumination pathway.<sup>29</sup> The authors of the latter work used a single water model and reported relatively high activation energies (>190 kJ/mol). We find significantly lower barriers ( $E_a = 114$ –157 kJ/mol, Table 3) due to significant differences from the reported mechanism. We find that the original protonated oxygen atom (BAS) is incorporated into the vicinal disilanol structure, while in ref 29, a nonprotonated framework oxygen is incorporated into the vicinal disilanol structure, bypassing C as intermediate. When the water molecule is coordinated to the Al atom in the *syn*-position, it is equally close to two framework oxygen atoms. The water proton moves toward one of framework oxygen atoms, while the water oxygen moves toward the other. Neither atom transfers across a large distance, and so water dissociation requires less energy. Moreover, the coordination of water to Al in C polarizes the water molecule, thus facilitating proton transfer.<sup>54</sup>

**Reactant C': 2  $\text{H}_2\text{O}$ .** The simultaneous adsorption of the  $\text{H}_2\text{O}^{(1)}$  in the *syn*-position to BAS and  $\text{H}_2\text{O}^{(2)}$  on the BAS proton allows to start the reaction according Mechanism III directly from adsorption mode C'. In the next step, the  $\text{H}_2\text{O}^{(1)}$  molecule (coordinated to the Al atom) is initially incorporated into the zeolite framework, forming a vicinal disilanol structure, while a proton is transferred to a neighboring framework oxygen (I2 +  $\text{H}_2\text{O}^{(2)}$ , Figure 8, right). This mechanism

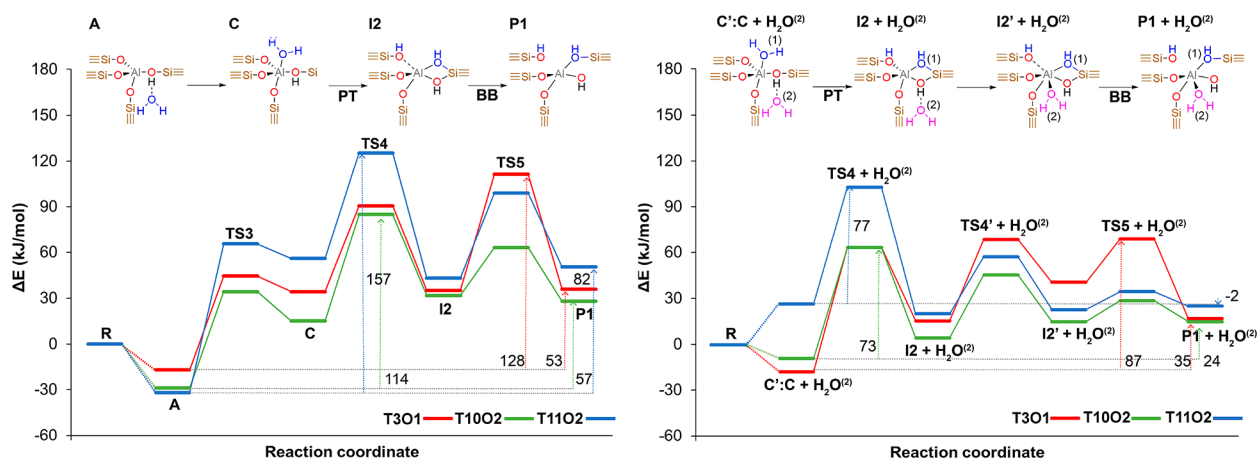


**Figure 8.** Reaction profile of Mechanism III in a single (left) and two water model (right). The Al–O(H) bond breaking follows proton transfer reaction (PT–BB) that occurs via formation of a vicinal disilanol intermediate (I2, I2 + H<sub>2</sub>O<sup>(2)</sup>, I2' + H<sub>2</sub>O<sup>(2)</sup>). Profiles are presented for three selected models with different Al positions: T3O1 (intersection), T10O2 (sinusoidal) and T11O2 (straight). R represents the empty zeolite, and its energy is corrected for a physisorbed water molecule.

**Table 3.** Adsorption Energies  $E_{\text{ads}}$ , the Reaction Energies  $\Delta E$ , the Activation Energies  $E_a$  (in kJ/mol) for the First Al–O(H) Bond Breaking According the Mechanism III<sup>a</sup>

Al location	adsorption mode	$E_{\text{ads}}$	$\Delta E$	$E_a$
T3O1 (inters.)	C	−17	53	128
	C'	−18	35	87
T10O2 (sinus.)	C	−29	57	114
	C'	−9	24	73
T11O2 (str.)	C	−32	82	157
	C'	27	−2	77

<sup>a</sup>Single and two water molecules models are compared.

involves an additional step, where H<sub>2</sub>O<sup>(2)</sup> moves to the Al atom, instigating an elongation of the Al–O(H) bond to the newly protonated oxygen and changing the coordination of the Al atom from penta-coordinated to trigonal bipyramidal (I2' + H<sub>2</sub>O<sup>(2)</sup>). Finally, the Al–O(H) bond is broken, while an O–Si bond in the vicinal disilanol structure also breaks and the product P1 is formed.

As discussed, Mechanism III requires three steps; (a) H<sub>2</sub>O<sup>(1)</sup> dissociation followed by O<sup>(1)</sup> insertion, (b) H<sub>2</sub>O<sup>(2)</sup> transfer, (c) Al–O(H) and O–Si bond breaking. The activation energies in the range of 73–87 kJ/mol are competitive with the barriers computed for Mechanism II, and the reaction is also thermodynamically favorable with reaction enthalpies ranging from −2 and 35 kJ/mol (Table 3). The energy barriers of the first step of the reaction (C' → I2 + H<sub>2</sub>O<sup>(2)</sup>) are rather insensitive toward the location of the Al site, as are the absolute stabilities of the first reaction intermediate (I2 + H<sub>2</sub>O<sup>(2)</sup>) and reaction product P1 + H<sub>2</sub>O<sup>(2)</sup> (Figure 8, right). The pathways diverge once the Al atom changes its coordination to trigonal bipyramidal (I2' + H<sub>2</sub>O<sup>(2)</sup>). The vicinal disilanol structure (I2 + H<sub>2</sub>O<sup>(2)</sup>, I2' + H<sub>2</sub>O<sup>(2)</sup>) introduces strain, and intermediate I2' has a rather distorted trigonal bipyramidal geometry, with a small H<sub>2</sub>O–Al–O(H) angle of 155° for the T3O1 Al site and 161° for the T10O2 and T11O2 Al site that causes steric repulsion (Figure 9). The amount of distortion is determined by the flexibility of the framework, and this affects the stabilities of TS4' + H<sub>2</sub>O<sup>(2)</sup>, I2' and TSS' + H<sub>2</sub>O<sup>(2)</sup>. As a result, these structures are affected very strongly by the position of Al site. Once the vicinal

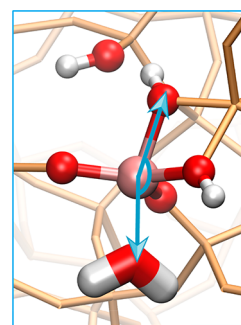


**Figure 9.** Intermediate I2' + H<sub>2</sub>O<sup>(2)</sup> of Mechanism III, which proceeds via formation of a vicinal disilanol structure. The Al atom has a distorted trigonal bipyramidal geometry with strained H<sub>2</sub>O–Al–O(H) angles ranging from 155 to 161°. The structure is shown for T3O1 site.

disilanol bonds are broken, the H<sub>2</sub>O–Al–O(H) angle can increase to 175° for T3O1 and T11O2 and 168° for T10O2; the strain is released, and the structures are stabilized, as can be seen from the comparable stabilities of the P1 + H<sub>2</sub>O<sup>(2)</sup> structures (Figure 8, right).

**Summary Mechanism III.** Analysis of the effect of the second water molecule reveals that the geometries of the intermediates do not change much, and both pathways are qualitatively similar. However, the additional water molecule lowers the activation energy by more than 40 kJ/mol for all Al sites. In the final step, the coordination of H<sub>2</sub>O<sup>(2)</sup> to the Al atom weakens the Al–O(H) bond, making it easier to break. This makes Mechanism III competitive with Mechanism II and demonstrates that the presence of multiple water molecules affects the mechanism of dealumination. All energies and structural data of Mechanism III for both water models are summarized in the Supporting Information (Tables S12–S16, Figures S6–S7).

**3.3.4. Mechanism IV: Spontaneous Al–O(H) Bond Breaking.** Our exhaustive testing of the stable adsorption modes of two water molecules show that mode C' results in an elongation of the Al–O(H) bond of up to 2.77–3.12 Å. This is about 1 Å longer than the Al–O(H) bond length in the unperturbed structure. We find that in this mode the Al–O(H) bond-breaking reaction can easily occur, via the straightforward

single-step process we have labeled as Mechanism IV (Figure 10).

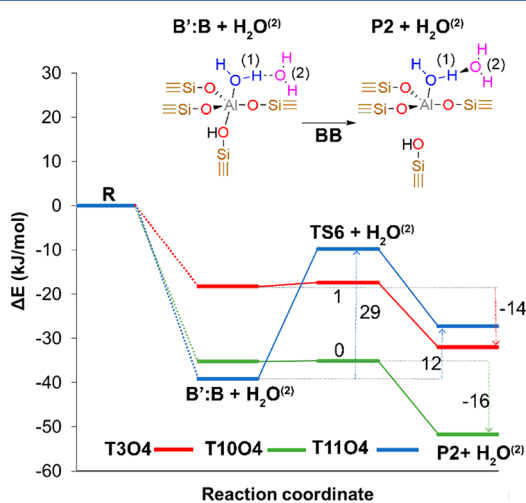


**Figure 10.** Mechanism IV: The simultaneous adsorption of both water molecules on the Al atom in the *anti*-position to the BAS proton ( $B'$ ) activates the Al–O(H) bond, resulting in straightforward bond breaking (BB). Profiles are presented for three selected models with different Al positions: T3O4 (intersection), T10O4 (sinusoidal), and T11O4 (straight). R represents the empty zeolite, and its energy is corrected for two physisorbed water molecules.

**Reactant  $B'$ : 2  $H_2O$ .** The energy barriers for the single step reaction are very low ( $E_a = 0\text{--}29$  kJ/mol) and can be overcome at room temperature. In the T3O4 and T10O4 models, Al–O(H) bond breaking occurs immediately, requiring almost no energy ( $E_a < 1$  kJ/mol) and the reactions are exothermic with  $\Delta E = -14$  and  $-16$  kJ/mol, respectively. The highest activation energy of 29 kJ/mol is required in the T11O4 model. Interestingly, this reaction is slightly endothermic ( $\Delta E = 12$  kJ/mol). Mechanism IV does not involve dissociation of either of the two water molecules, and therefore, its product P2 differs from the products of Mechanisms I–III (P1). The Al atom in product P2 is bonded to three framework oxygen atoms and a water molecule and has a distorted tetrahedral geometry (Figure 10). Experimental evidence of such a distorted tetrahedral species has been reported.<sup>25,55,56</sup> The thermodynamic stability of P2 is higher than that of the most stable forms of P1 by 73, 67, and 53 kJ/mol in the T3, T10, and T11 models, respectively. The stability of P2 depends on the Al and BAS position. We identified this state only in the T3O2, T3O4, T10O4, and T11O4 models. Tabulated energies and structural data of Mechanism IV are summarized in the Supporting Information (Tables S17–S18, Figure S8).

**Summary Mechanism IV.** We found that the formation of P2 is much easier than the formation of P1 via any of the proposed mechanisms and that P2 is thermodynamically more stable than P1. This effect is strongest in the sinusoidal pore (T10 model) and at intersection (T3 model), while an Al atom in the straight pore (T11 model) is least likely to break a bond to an oxygen atom. However, to form a free EFAL species, the novel reaction product P2 initiates a different dealumination mechanism shown in Scheme 4, which will require further investigation in the future. Alternatively, the P2 product may be a reactant in Mechanism I and II, effectively lowering the reaction barriers.

**3.3.5. Comparing the Four Mechanisms.** All activation energies ( $E_a = E_{\ddagger}^{\max} - E_{\text{reactant}}$ ) reported and compared thus far are with respect to the corresponding reactant, which is one of the active adsorption modes (reactant A', B' or C'). For the sake of comparison, we now assume that the reactant states are equally easy to form, through facile rearrangement of the water in the system. The reliability of this comparison will be addressed in the Section 3.4. Using this assumption, we find the highest activation energies for Mechanism I, in which the second water molecule only contributes to the reaction indirectly (I:  $E_a = 102\text{--}120$  kJ/mol, Table 4). Mechanisms

**Table 4. Summarized Activation Energies  $E_a$  (in kJ/mol) for All Proposed Reaction Pathways of the First Al–O(H) Bond Breaking, with Respect to the Starting (Active) Adsorption Mode**

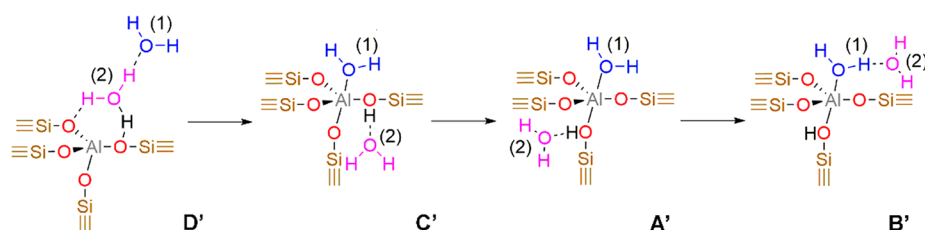
mechanism	$E_a = E_{\ddagger}^{\max} - E_{\text{reactant}}$			
	I	II	III	IV
Al location				
T3 (inters.)	102	80	87	1
T10 (sinus.)	102	78	73	0
T11 (str.)	120	87	77	29

II and III, in which the second water molecule actively participates, yield much lower barriers (II:  $E_a = 78\text{--}87$  kJ/mol, III:  $E_a = 73\text{--}87$  kJ/mol, Table 4). The latter two mechanisms have activation energies in the same range, and neither of them stands out as the more likely pathway. Mechanism IV yields a different type of product than the other mechanisms (P2), but it is kinetically and thermodynamically the most favorable. The reaction occurs spontaneously in the T3O4 and T10O4 Al models, while the modest barrier of 29 kJ/mol (with respect to the  $B'$ :  $B+H_2O^{(2)}$  intermediate) must be overcome in the T11O4 model. Because this mechanism has significantly lower barriers, it can be expected to be the most likely first step of the dealumination process. However, this conclusion assumes that formation of an EFAL species from product P2 is not more energy consuming than the formation of EFAL from the product P1.

Irrespective of this assumption, we find that the sinusoidal channel (T10 model) is the most reactive for each of the Mechanisms I–IV, with the lowest activation energies (I:  $E_a = 102$  kJ/mol, II:  $E_a = 78$  kJ/mol, III:  $E_a = 73$ , IV:  $E_a = 0$  kJ/mol). Mechanism IV predicts that the straight channel (T11 model) is the least reactive with  $E_a = 29$  kJ/mol. If Mechanism IV is not a viable route toward EFAL formation, then our results suggest that the Al atom located in the intersection is the most stable (II:  $E_a = 80$  kJ/mol). In contrast, a single water molecule model predicts T3 site (intersection) as the most reactive Al site ( $E_a = 86$  kJ/mol), while T10 and T11 sites are much stable ( $E_a = 103$  kJ/mol). This indicates that the Al site reactivity can be altered by varying water loading during a steaming period for the postsynthetic zeolite treatment to tune Al distribution.

Although the four mechanisms are very different, a common feature is the coordination of a water molecule to the Al atom (either in *syn*- or *anti*-position). This is in agreement with previous reports,<sup>30,57</sup> which state that the coordination of the water to the Al is crucial for the bond-breaking reaction. We have thus far assumed that the reactant modes are equally accessible for all three sites, but that assumption does require further scrutiny. The following sections therefore addresses the

**Scheme 5. Reorganization of Water Molecules from the Most Stable Mode D' into One of the Active Adsorption Modes (B', A', or C')<sup>a</sup>**



<sup>a</sup>The reaction scheme shows the energetically most favorable mechanism.

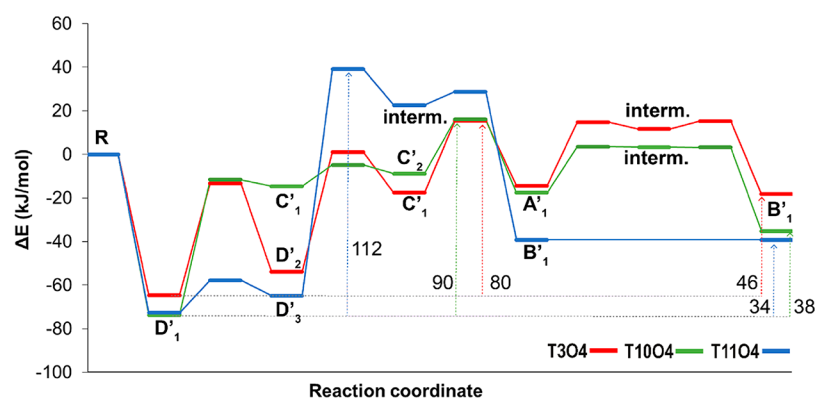


**Figure 11.** Energy profiles for the reorganization of water molecules from the most stable and unreactive Zundel ion D' into the reactive adsorption mode C' for the three selected models T3O4 (intersection), T10O4 (sinusoidal), and T11O4 (straight). R represents the empty zeolite, and its energy is corrected for two physisorbed water molecules.

effect of the accessibility of the reactant modes on the relative stabilities of the different ZSM-5 active sites.

**3.4. Water Rearrangement to the Active Adsorption Modes.** Because dealumination cannot be initiated from the most stable mode D' directly, it must be preceded by water rearrangement into one of the active adsorption modes. In this subsection, we address the energy cost of the water reorganization required for the formation of an active adsorption mode, and how this affects the relative probabilities of the mechanisms discussed in the previous section. Starting from the most stable configuration, Zundel ion D', we find that energetically, the most favorable is the rearrangement to B' via C' and A' (Scheme 5). First, the D' dimer dissociates, while the excess proton transfers to the *syn*-framework oxygen, forming C'. The second step involves a transfer of the proton to the *anti*-position via H<sub>2</sub>O<sup>(2)</sup>, forming adsorption mode A'. Finally, H<sub>2</sub>O<sup>(2)</sup> desorbs from the BAS proton and moves toward H<sub>2</sub>O<sup>(1)</sup> to form B'. This process sometimes involves a metastable intermediate in which H<sub>2</sub>O<sup>(2)</sup> is weakly physisorbed to zeolite framework. Example energy profiles for the reorganization process for the three selected models (Mechanism IV, T3O4, T10O4, and T11O4) are depicted in Figure 11. The second step, rearrangement from C' to A', is the rate-determining step and includes the movement of BAS proton between framework oxygen atoms via water molecule H<sub>2</sub>O<sup>(2)</sup>, which causes the transformation of the *syn*-position to the *anti*-position to the BAS. Out of these selected models, the lowest activation energy with respect to reactant D' of 80 kJ/mol is obtained for T3O4, which is expected; the Al atom in the intersection is presumably the most accessible, making the reorientation of water molecules easy. The proposed reaction scheme is more favorable than direct reorganization from D' to

A', because the latter involves water transfer across larger distances. Similarly, the direct conversion from D' to B' is not likely to be energetically favorable as it is easier to decompose a Zundel ion H<sub>3</sub>O<sub>2</sub><sup>+</sup> into H<sub>3</sub>O<sup>+</sup> and H<sub>2</sub>O than into 2 H<sub>2</sub>O and H<sup>+</sup>.

The T11O4 model forms an exception to this rearrangement mechanism. In mode A', the two water molecules are adsorbed in different channels, and therefore, there is no feasible mechanism for reorganization from D' to A'. Consequently, mode B' can be formed only by direct decomposition of D'. This reorganization has an activation energy of 112 kJ/mol with respect to mode D'. All reorganization pathways for each of the proposed Mechanism I–IV are listed in the Supporting Information (Tables S19–S21).

**3.5. Overall Reactivity.** As discussed in Section 3.4, all Al–O(H) bond-breaking reactions must be preceded by water rearrangement, presumably from the most stable adsorption mode D' to one of the active adsorption modes (A', B', C'; Scheme 5). Including this process in our analysis of the relative Al–O(H) bond-breaking probabilities should provide a more exact picture, within the constraints of our model. In this section, we discuss the activation energies for the full reaction pathways (including water reorganization and Al–O(H) bond breaking) with respect to mode D' as the reactant ( $E_a^{D'} = E_a^{\ddagger} - E_{D'}$ ). Water rearrangement is not the rate-determining process for Mechanisms I–III (Table 5), while for Mechanism IV it is. Mechanism IV remains the easiest overall pathway for hydrolysis of the Al–O(H) bond, regardless of Al location. Mechanism II is now preferred over Mechanism III ( $\Delta E_a^{D'} = 0$ –37 kJ/mol), while Mechanism I is the least probable pathway.

At all three Al sites (T3O4, T10O1 and T11O4), Mechanism II presents the most favorable pathway of type

**Table 5. Summarized Effective Barriers (in kJ/mol) for All Proposed Reaction Pathways of the First Al–O(H) Bond Breaking, with Respect to the Most Stable Adsorption Mode: a Zundel Ion (D')**

mechanism	$E_a^{D'} = E_{\max}^{\ddagger} - E_{D'}$			
	I	II	III	IV
T3 (inters.)	148	134	134	80
T10 (sinus.)	156	122	137	90
T11 (str.)	159	139	176	112

PT-BB, with  $E_a^{D'}$  values of 134 kJ/mol, 122 and 139 kJ/mol respectively; the T10 model is still the most reactive, while the T3 and T11 models still exhibit similar reactivity (Mechanism II, Table 5). If we assume that Mechanism IV is a viable pathway toward a free EFAL species, then water rearrangements has a considerable effect on the results. It is no longer the Al atom in the sinusoidal channel that is most reactive, but now it is the Al atom at the intersection (T3:  $E_a^{D'}=80$  kJ/mol). The straight channel remains the least reactive Al location (T11:  $E_a^{D'}=112$  kJ/mol). Strikingly, within the constraints of our model, the rearrangement of water to a reactive conformation may be a determining factor in the stability of an Al site against dealumination.

**3.6. Free Energy Corrections.** Thus far, all reported energies are pure potential energies at 0 K. In this section, we discuss the effect of realistic conditions on the reaction profiles. At first, we illustrate the effect of corrections for zero-point

energy (ZPE), pressure, and entropy on new reaction mechanisms for two water model at single temperature of 450 K, the temperature that corresponds to mild steaming conditions.<sup>58</sup> In the next step, the preference of the different reaction pathways more generally, for a wide range of reaction conditions, is addressed.

**3.6.1. Free Energy Profiles at 450 K.** The analysis of free energy profiles at 450 K reveals that the ZPE and finite temperature corrections affects mainly the adsorption energies because of the loss of translational and rotational degrees of freedom upon adsorption, which results in a reduction of all barrier heights. Nonetheless, Mechanism IV is still the preferred mechanism for all the models (T3:  $G^{\ddagger} = 66$  kJ/mol, T10:  $G^{\ddagger} = 71$  kJ/mol, T11:  $G^{\ddagger} = 86$  kJ/mol). Mechanism II remains the second most probable pathway (T3:  $G^{\ddagger} = 117$  kJ/mol, T10:  $G^{\ddagger} = 106$  kJ/mol, T11:  $G^{\ddagger} = 103$  kJ/mol), while the Mechanism III is still a feasible alternative, particularly for T3 and T10 Al site ( $G^{\ddagger} = 125$  and 116 kJ/mol). The obtained free energy profiles at 450 K, including water rearrangement as well as Al–O(H) bond breaking, can be found in Supporting Information (Figure S9, Tables S22–S28).

While a water reorganization is still not rate-determining for Mechanism I–III, the difference between the activation energies for Al–O(H) bond breaking ( $E_a$ ) and for water reorganization ( $E_a^w$ ) are smaller at 450 K than at 0 K (Figure S9). In the example of Mechanism II (the most favorable of the three PT-BB reactions), the difference between the two activation energies is reduced from 54 to 50 kJ/mol in the T3O4 model, from 13 to 12 kJ/mol in the T10O1 model, and from 27 to 17 kJ/mol in the T11O4 model. Extrapolation of

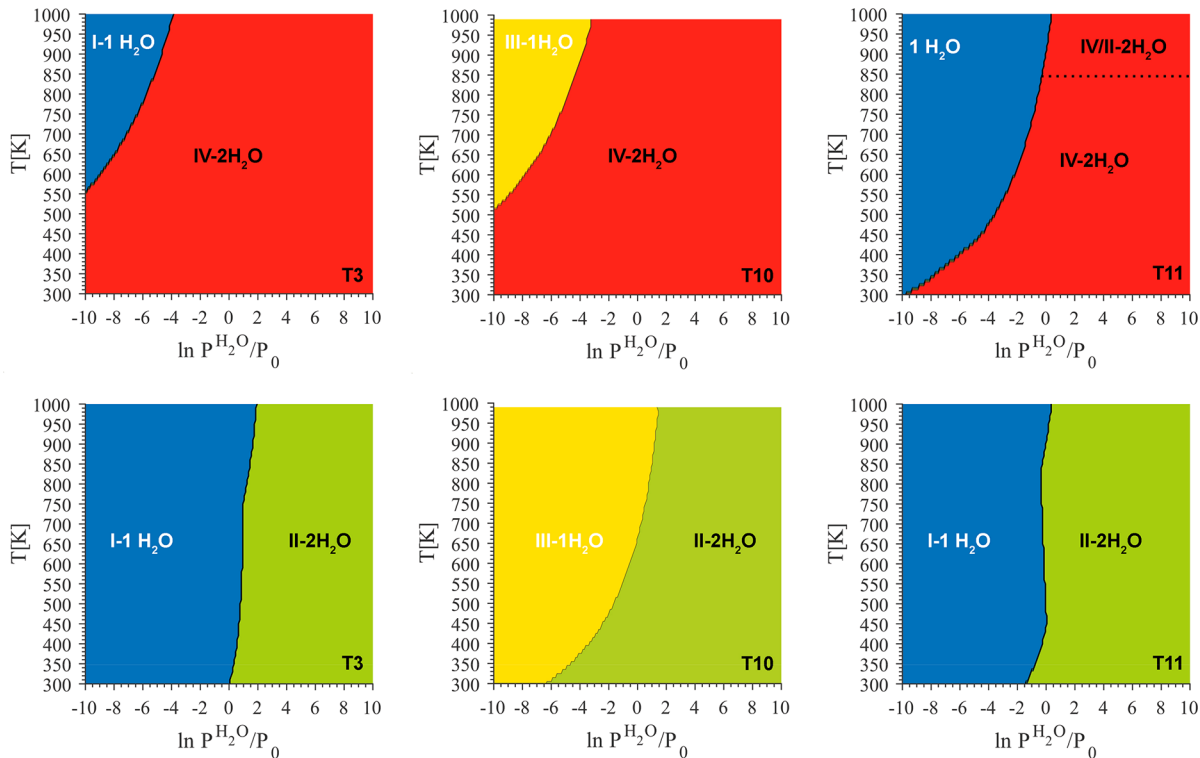


**Figure 12.** Phase diagrams for the preferred dealumination mechanisms at various temperatures and water pressures for different Al sites including all mechanisms (top) or excluding Mechanism IV (bottom). Blue regions represent Mechanism I for a single water model, green regions correspond to Mechanism II, yellow regions to Mechanism III for a single water model, and red regions correspond to Mechanism IV. For T11 site (top right), we identify a region of high  $T$  and  $p_{H_2O}$ , where Mechanism II and Mechanism IV occurs with the same probability. At these conditions the energy cost of water reorganization of both reactions is higher than the Al–O(H) bond breaking itself.

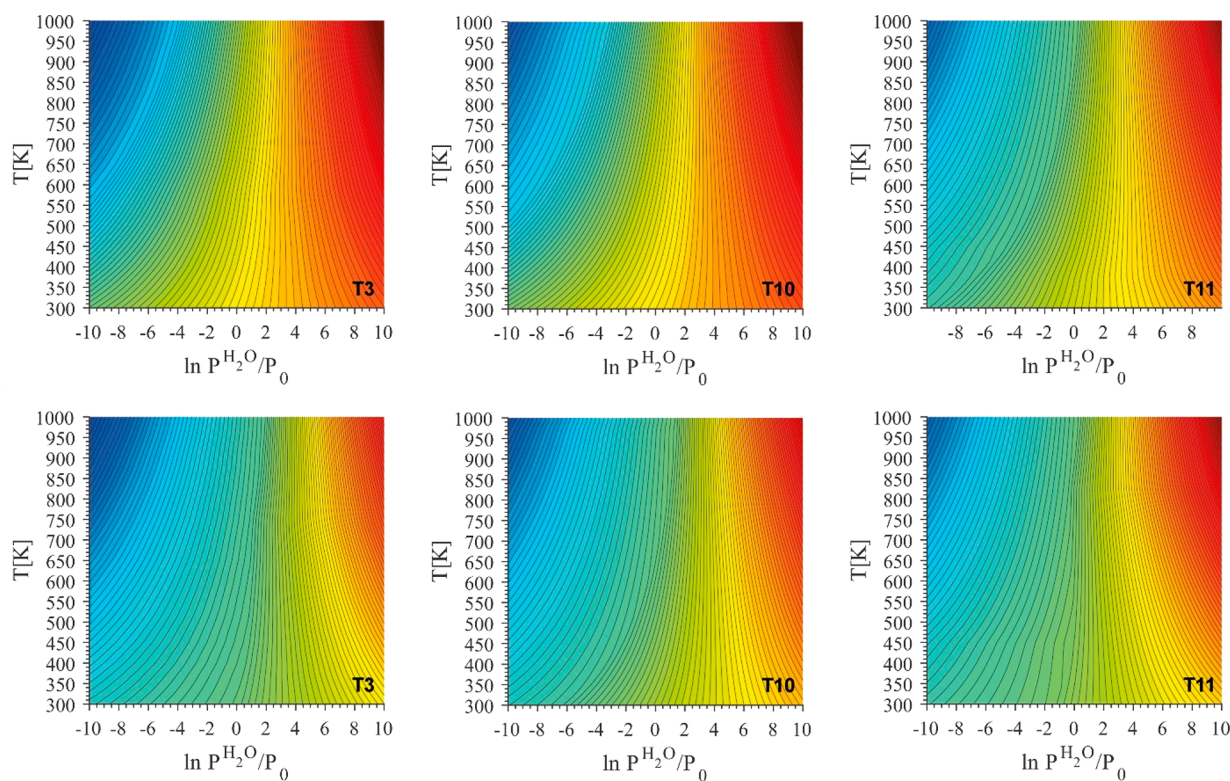


**Figure 13.** Phase diagram for  $-\frac{C^{\ddagger, \max}}{k_B T}$  for the three different Al sites: T3 (intersection), T10 (sinusoidal), and T11 (straight). The lowest rates correspond to blue regions and highest rates correspond to red regions. The diagrams are shown for the situation where all reaction mechanisms are considered (top) as well as when Mechanism IV is excluded (bottom). The diagrams show that the relative susceptibility of Al site toward the first Al–O(H) bond breaking depends on the reaction conditions.

our results to temperatures of severe steaming<sup>26</sup> suggests that under those conditions water reorganization will have similar energy requirements as the Al–O(H) bond-breaking reaction. This agrees with the findings of Agostini et al., who showed that at high temperatures the free energy cost of the water adsorption might become critical<sup>58</sup> and advocates the hypothesis put forward in Section 3.3.2 that the accessibility of the active site is one of the main factors determining the reactivity of the Al site. It has to be emphasized that the energy profiles presented here are based on static calculations using harmonic approximation that might not accurately describe the entropic contribution to the free energy of highly mobile species, particularly Zundel ion (D'). As a result, the free energy difference between initial state D' and active adsorption modes A'–C' is underestimated, which further supports our conclusion that the water reorganization affects the kinetics of the dealumination. The accurate evaluation of free energy differences between adsorption states requires performing a set of molecular dynamics simulations with enhanced sampling, which should be further explored in the future.

**3.6.2. Impact of Dealumination Conditions.** To explore how the preference of the different reaction pathways and the susceptibility of Al sites toward the first Al–O(H) bond breaking depends on realistic conditions, we modeled the reaction activities and phase diagrams between 300 and 1000 K and partial water pressures between  $e^{-10}$  and  $e^{10}$  bar.

In Figure 12 we show  $T, p_{\text{H}_2\text{O}}$  phase diagrams of the preferred mechanisms with water reorganization included. We find that for all Al sites, the phase diagrams are dominated by Mechanism IV with two water molecules adsorbed in position

B'. For all three Al sites, we find a region at high  $T$  and low  $p_{\text{H}_2\text{O}}$  where a dealumination mechanism starting from a single adsorbed water molecule is preferred. The increase in size of this region for T11 agrees with the previous observation that it is the least accessible, which makes adsorption of multiple water molecules more difficult. For T11 site at conditions corresponding to a high  $T$  and  $p_{\text{H}_2\text{O}}$ , we identify a region, where Mechanism II and Mechanism IV occurs simultaneously, with the same barriers. At these conditions, the rate-determining step of both reactions is the water reorganization from D' to B'. However, subsequent Al–O(H) bond breaking of Mechanism IV requires less energy, and therefore, we assume that under these conditions Mechanism IV will be prevalent as well. Additionally, we are interested in the next most likely mechanisms, besides Mechanism IV (Figure 12, bottom). We see that for all three Al sites, a mechanism starting from a single water molecule model is prevalent at  $p_{\text{H}_2\text{O}} < 1$  atm across all  $T$ , while the two-water molecule model is preferred when  $p_{\text{H}_2\text{O}} > 1$  atm.

In the next step, we estimated the condition-dependent reaction rates. Since we are mainly interested in trends, we omit the inclusion of pre-exponential factor in the reaction rate and explore only the temperature dependence of the  $-\frac{C^{\ddagger, \max}}{k_B T}$  factor as shown in Figure 13. We find that for conditions typically found in gas phase reactions, where  $p_{\text{H}_2\text{O}} \ll 1$  bar, an increase in temperature leads to a decrease in dealumination rate. We attribute this behavior to the loss of water molecules close to the Al site under these conditions. The reaction rate

can be increased by increasing  $p_{\text{H}_2\text{O}}$ , which is consistent with experimental observation, where steaming, that is, the increase in  $p_{\text{H}_2\text{O}}$  at higher temperatures, is used to dealuminate zeolites. Additionally, we find that in the region dominated by a single water model corresponding to high  $T$  and low  $p_{\text{H}_2\text{O}}$  the initial Al–O(H) bond breaking is the easiest for Al site in the straight channel (T11), followed by the sinusoidal channel (T10) and intersection (T3). Different behavior is observed for regions at  $p_{\text{H}_2\text{O}} > 1$  atm and all  $T$ . If we assume that Mechanism IV is the viable pathway toward the free EFAL species, then the Al site in the straight channel (T11) shows the highest stability, while Al located in the sinusoidal channel (T10) is the most reactive toward the Al–O(H) bond breaking with the rate-determining step being water reorganization. This agrees with the observations from Section 3.1.2, in which the Al site in the straight channel is the least accessible for water adsorption. If we exclude Mechanism IV from the analysis, we observe the same trends except for the regions of high  $T$  and  $p_{\text{H}_2\text{O}}$ , where Al in the straight channel (T11) is the least stable toward the initial Al–O(H) bond breaking followed by the intersection (T3) and sinusoidal channel (T10). On the basis of the analysis of reaction rates, we can conclude that the susceptibility of Al sites toward dealumination depends on the reaction conditions. This observation might explain the discrepancy between the findings of Karwacki et al.,<sup>24</sup> who assigned Al located in the sinusoidal as the most susceptible toward dealumination, while Holzinger et al.<sup>25</sup> found Al located in the intersection as the least stable. Moreover, on the basis of the analysis of phase diagrams and reactivities, we can further support the hypothesis that Al distribution can be systematically altered by applying the steaming at various reaction conditions as postsynthetic treatment.

To elucidate the influence of dispersion interactions on the reaction profiles, we have recomputed the phase diagrams with -D2 corrections as described in Methods. The results are shown in Supporting Information (Figures S10–S11). We find, that the inclusion of the dispersion corrections is the decisive factor when comparing the prevalence of a single versus two water molecule model; however, it does not affect the relative Al site stabilities. Compared to the  $p, T$  diagrams in Figure 12, the two water molecule model is preferred for a bigger range of conditions, including the region of low  $T$  and  $p_{\text{H}_2\text{O}}$ , where a single water model is favored if the dispersion corrections are omitted (Figure S10). Interestingly, for the Al site in the intersection (T3), we find that with -D2 corrections, Mechanism III becomes the most favorable for high  $p_{\text{H}_2\text{O}}$  and low  $T$ , proving that multiple dealumination pathways are feasible. When comparing the activities (Figure 13 and Figure S11), the inclusion of dispersion corrections leads to higher reaction rates due to the systematic lowering of the free energies of all states. However, the dispersion corrections do not qualitatively affect the reactivities of Al sites and we observe the same trends across all reaction conditions for both PBE and PBE-D2 functional.

## 4. CONCLUSIONS

Our study of the initial stage of the water-induced dealumination in a ZSM-5 zeolite model containing two water molecules explores the role of water–water interactions on the reactions. By including two explicit water molecules into our

system, we show that microsolvation alters the dealumination reaction mechanism as well as its energetics. We identify four different mechanisms for the Al–O(H) bond-breaking reaction, each initiated from a different active adsorption mode. Mechanism I is identical to a previously reported mechanism that was found using a single-water model.<sup>30</sup> Mechanism II is very similar, but it allows proton transfer across multiple water molecules and hence effectively lowers the reaction barriers. In Mechanism III, the water molecule is temporarily incorporated into the zeolite framework prior to Al–O(H) bond breaking. Mechanism IV is thermodynamically and kinetically preferred and involves spontaneous Al–O(H) bond breaking due to coordination of the water molecules at the Al atom in the *anti*-position to the BAS. This yields a different product, suggesting an alternative follow-up dealumination route than proposed in previous works. Within ZSM-5 zeolite model, we establish a direct link between a reaction conditions and the susceptibility of Al site toward dealumination. At reaction conditions corresponding to high  $T$  and low  $p_{\text{H}_2\text{O}}$  at which a single water molecule model is prevalent, we find that the Al located in the intersection (T3) is the least reactive toward the first Al–O(H) bond breaking. If we assume that the novel Mechanism IV provides the most viable route to free Al species, then at conditions of increased  $p_{\text{H}_2\text{O}}$  that are relevant for zeolite steaming the Al site in the straight channel (T11) shows the highest stability, with the rate determine step being water reorganization. We find that the regioselectivity of Al sites during dealumination is not determined by the stability of the Al–O(H) bond, but rather by the accessibility and the solvation of the active Al site and temperature. We suggest that pressure-controlled dealumination can be used as a postsynthetic treatment to manufacture hydrothermally stable and reactive zeolite catalysts.

## ■ ASSOCIATED CONTENT

### 📄 Supporting Information

The Supporting Information is available free of charge on the ACS Publications website at DOI: 10.1021/acscatal.9b00307.

Additional data including adsorption energies, recalculations using PBE+D2 functional, tabulated adsorption energies, Mechanism I for a single water molecule model, phase diagrams with D2 corrections, and other supporting data as indicated in the text (PDF)

## ■ AUTHOR INFORMATION

### Corresponding Authors

\*E-mail: B.M.Weckhuysen@uu.nl.

\*E-mail: R.E.Bulo@vu.nl.

### ORCID

Bert M. Weckhuysen: 0000-0001-5245-1426

### Present Address

<sup>1</sup>R.E.B.: Department of Theoretical Chemistry, Vrije Universiteit Amsterdam, De Boelelaan 1083, 1081 HV Amsterdam, The Netherlands

### Notes

The authors declare no competing financial interest.

## ■ ACKNOWLEDGMENTS

This work was supported by The Netherlands Center for Multiscale Catalytic Energy Conversion (MCEC), an NWO Gravitation program funded by the Ministry of Education,



Culture and Science of the government of The Netherlands. The authors also thank The Netherlands Organization for Scientific Research (NWO) for access to the national high-performance computing facilities. Florian Göttl acknowledges support within the National Science Foundation grant CHE-1800284.

## REFERENCES

- (1) Yilmaz, B.; Müller, U. Catalytic Applications of Zeolites in Chemical Industry. *Top. Catal.* **2009**, *52*, 888–895.
- (2) Wang, S.; Peng, Y. Natural Zeolites as Effective Adsorbents in Water and Wastewater Treatment. *Chem. Eng. J.* **2010**, *156*, 11–24.
- (3) Vogt, E. T. C.; Weckhuysen, B. M. Fluid Catalytic Cracking: Recent Developments on the Grand Old Lady of Zeolite Catalysis. *Chem. Soc. Rev.* **2015**, *44*, 7342–7370.
- (4) Ono, Y. Transformation of Lower Alkanes into Aromatic Hydrocarbons over ZSM-5 Zeolites. *Catal. Rev.: Sci. Eng.* **1992**, *34*, 179–226.
- (5) Stöcker, M. Methanol-to-Hydrocarbons: Catalytic Materials and Their Behavior. *Microporous Mesoporous Mater.* **1999**, *29*, 3–48.
- (6) Olsbye, U.; Svelle, S.; Bjørgen, M.; Beato, P.; Janssens, T. V. W.; Joensen, F.; Bordiga, S.; Lillerud, K. P. Conversion of Methanol to Hydrocarbons: How Zeolite Cavity and Pore Size Controls Product Selectivity. *Angew. Chem., Int. Ed.* **2012**, *51*, 5810–5831.
- (7) Carlson, T. R.; Tompsett, G. A.; Conner, W. C.; Huber, G. W. Aromatic Production from Catalytic Fast Pyrolysis of Biomass-Derived Feedstocks. *Top. Catal.* **2009**, *52*, 241–252.
- (8) Taarning, E.; Osmundsen, C. M.; Yang, X.; Voss, B.; Andersen, S. I.; Christensen, C. H. Zeolite-Catalyzed Biomass Conversion to Fuels and Chemicals. *Energy Environ. Sci.* **2011**, *4*, 793–804.
- (9) van Donk, S.; Janssen, A. H.; Bitter, J. H.; de Jong, K. P. Generation, Characterization, and Impact of Mesopores in Zeolite Catalysts. *Catal. Rev.: Sci. Eng.* **2003**, *45*, 297–319.
- (10) Triantafyllidis, C. S.; Vlessidis, A. G.; Evmiridis, N. P. Dealuminated H–Y Zeolites: Influence of the Degree and the Type of Dealumination Method on the Structural and Acidic Characteristics of H–Y Zeolites. *Ind. Eng. Chem. Res.* **2000**, *39*, 307–319.
- (11) Triantafyllidis, C. S.; Vlessidis, A. G.; Nalbandian, L.; Evmiridis, N. P. Effect of the Degree and Type of the Dealumination Method on the Structural, Compositional and Acidic Characteristics of H-ZSM-5 Zeolites. *Microporous Mesoporous Mater.* **2001**, *47*, 369–388.
- (12) Lopez-Orozco, S.; Inayat, A.; Schwab, A.; Selvam, T.; Schwiager, W. Zeolitic Materials with Hierarchical Porous Structures. *Adv. Mater.* **2011**, *23*, 2602–2615.
- (13) Song, S.; Di, L.; Wu, G.; Dai, W.; Guan, N.; Li, L. Meso-Zr-Al-Beta Zeolite as a Robust Catalyst for Cascade Reactions in Biomass Valorization. *Appl. Catal., B* **2017**, *205*, 393–403.
- (14) Zhao, R.; Zhao, Z.; Li, S.; Parvulescu, A.-N.; Müller, U.; Zhang, W. Excellent Performances of Dealuminated H-Beta Zeolites from Organotemplate-Free Synthesis in Conversion of Biomass-Derived 2,5-Dimethylfuran to Renewable *p*-Xylene. *ChemSusChem* **2018**, *11*, 3803–3811.
- (15) Corma, A.; Mengual, J.; Miguel, P. J. Steam Catalytic Cracking of Naphtha over ZSM-5 Zeolite for Production of Propene and Ethene: Micro and Macroscopic Implications of the Presence of Steam. *Appl. Catal., A* **2012**, *417–418*, 220–235.
- (16) Yang, H.; Coolman, R. J.; Karanjkar, P.; Wang, H.; Xu, Z.; Chen, H.; Moutziaris, T. J.; Huber, G. W. The Effect of Steam on the Catalytic Fast Pyrolysis of Cellulose. *Green Chem.* **2015**, *17*, 2912–2923.
- (17) Gayubo, A. G.; Aguayo, A. T.; Atutxa, A.; Prieto, R.; Bilbao, J. Deactivation of a HZSM-5 Zeolite Catalyst in the Transformation of the Aqueous Fraction of Biomass Pyrolysis Oil into Hydrocarbons. *Energy Fuels* **2004**, *18*, 1640–1647.
- (18) Wu, X.; Anthony, R. G. Effect of Feed Composition on Methanol Conversion to Light Olefins over SAPO-34. *Appl. Catal., A* **2001**, *218*, 241–250.
- (19) De Wispelaere, K.; Wondergem, C. S.; Ensing, B.; Hemelsoet, K.; Meijer, E. J.; Weckhuysen, B. M.; Van Speybroeck, V.; Ruiz-Martinez, J. Insight into the Effect of Water on the Methanol-to-Olefins Conversion in H-SAPO-34 from Molecular Simulations and in Situ Microspectroscopy. *ACS Catal.* **2016**, *6*, 1991–2002.
- (20) Iliopoulou, E. F.; Stefanidis, S.; Kalogiannis, K.; Psarras, A. C.; Delimitis, A.; Triantafyllidis, K. S.; Lappas, A. A. Pilot-Scale Validation of Co-ZSM-5 Catalyst Performance in the Catalytic Upgrading of Biomass Pyrolysis Vapours. *Green Chem.* **2014**, *16*, 662–674.
- (21) Vitolo, S.; Bresci, B.; Seggiani, M.; Gallo, M. G. Catalytic Upgrading of Pyrolytic Oils over HZSM-5 Zeolite: Behaviour of the Catalyst When Used in Repeated Upgrading-Regenerating Cycles. *Fuel* **2001**, *80*, 17–26.
- (22) Gayubo, A. G.; Aguayo, A. T.; Olazar, M.; Vivanco, R.; Bilbao, J. Kinetics of the Irreversible Deactivation of the HZSM-5 Catalyst in the MTO Process. *Chem. Eng. Sci.* **2003**, *58*, 5239–5249.
- (23) Ong, L. H.; Dömök, M.; Olindo, R.; Van Veen, A. C.; Lercher, J. a. Dealumination of HZSM-5 via Steam-Treatment. *Microporous Mesoporous Mater.* **2012**, *164*, 9–20.
- (24) Karwacki, L.; de Winter, D. A. M.; Aramburo, L. R.; Lebbink, M. N.; Post, J. A.; Drury, M. R.; Weckhuysen, B. M. Architecture-Dependent Distribution of Mesopores in Steamed Zeolite Crystals as Visualized by FIB-SEM Tomography. *Angew. Chem., Int. Ed.* **2011**, *50*, 1294–1298.
- (25) Holzinger, J.; Beato, P.; Lundegaard, L. F.; Skibsted, J. Distribution of Aluminum over the Tetrahedral Sites in ZSM-5 Zeolites and Their Evolution after Steam Treatment. *J. Phys. Chem. C* **2018**, *122*, 15595–15613.
- (26) Perea, D. E.; Arslan, I.; Liu, J.; Ristanović, Z.; Kovarik, L.; Arey, B. W.; Lercher, J. A.; Bare, S. R.; Weckhuysen, B. M. Determining the Location and Nearest Neighbours of Aluminium in Zeolites with Atom Probe Tomography. *Nat. Commun.* **2015**, *6*, 1–8.
- (27) Ruetter, F.; Sánchez, M.; Martorell, G.; González, C.; Añez, R.; Sierralta, A.; Rincón, L.; Mendoza, C. CATIVIC: Parametric Quantum Chemistry Package for Catalytic Reactions: I. *Int. J. Quantum Chem.* **2004**, *96*, 321–332.
- (28) Lisboa, O.; Sánchez, M.; Ruetter, F. Modeling Extra Framework Aluminum (EFAL) Formation in the Zeolite ZSM-5 Using Parametric Quantum and DFT Methods. *J. Mol. Catal. A: Chem.* **2008**, *294*, 93–101.
- (29) Malola, S.; Svelle, S.; Bleken, F. L.; Swang, O. Detailed Reaction Paths for Zeolite Dealumination and Desilication from Density Functional Calculations. *Angew. Chem., Int. Ed.* **2012**, *51*, 652–655.
- (30) Silaghi, M.; Chizallet, C.; Petracovschi, E.; Kerber, T.; Sauer, J.; Raybaud, P. Regioselectivity of Al–O Bond Hydrolysis during Zeolites Dealumination Unified by Brønsted–Evans–Polanyi Relationship. *ACS Catal.* **2015**, *5*, 11–15.
- (31) Silaghi, M.-C.; Chizallet, C.; Sauer, J.; Raybaud, P. Dealumination Mechanisms of Zeolites and Extra-Framework Aluminum Confinement. *J. Catal.* **2016**, *339*, 242–255.
- (32) Fjermestad, T.; Svelle, S.; Swang, O. Mechanistic Comparison of the Dealumination in SSZ-13 and the Desilication in SAPO-34. *J. Phys. Chem. C* **2013**, *117*, 13442–13451.
- (33) Fjermestad, T.; Svelle, S.; Swang, O. Desilication of SAPO-34: Reaction Mechanisms from Periodic DFT Calculations. *J. Phys. Chem. C* **2015**, *119*, 2073–2085.
- (34) Valdiviés-Cruz, K.; Lam, A.; Zicovich-Wilson, C. M. Full Mechanism of Zeolite Dealumination in Aqueous Strong Acid Medium: Ab Initio Periodic Study on H-Clinoptilolite. *J. Phys. Chem. C* **2017**, *121*, 2652–2660.
- (35) van Koningsveld, H.; Jansen, J.; van Bekkum, H. The Monoclinic Framework Structure of Zeolite H-ZSM-5. Comparison with the Orthorhombic Framework of as-Synthesized ZSM-5. *Zeolites* **1990**, *10*, 235–242.
- (36) Hutter, J.; Iannuzzi, M.; Schiffrmann, F.; VandeVondele, J. Cp2k: Atomistic Simulations of Condensed Matter Systems. *Wiley Interdiscip. Rev. Comput. Mol. Sci.* **2014**, *4*, 15–25.

- (37) VandeVondele, J.; Krack, M.; Mohamed, F.; Parrinello, M.; Chassaing, T.; Hutter, J. Quickstep: Fast and Accurate Density Functional Calculations Using a Mixed Gaussian and Plane Waves Approach. *Comput. Phys. Commun.* **2005**, *167*, 103–128.
- (38) Perdew, J. P.; Burke, K.; Ernzerhof, M. Generalized Gradient Approximation Made Simple. *Phys. Rev. Lett.* **1996**, *77*, 3865–3868.
- (39) Fischer, M. Structure and Bonding of Water Molecules in Zeolite Hosts: Benchmarking Plane-Wave DFT against Crystal Structure Data. *Z. Kristallogr. - Cryst. Mater.* **2015**, *230*, 325–336.
- (40) Grimme, S. Semiempirical GGA-Type Density Functional Constructed with a Long-Range Dispersion Correction. *J. Comput. Chem.* **2006**, *27*, 1787–1799.
- (41) Nielsen, M.; Brogaard, R. Y.; Falsig, H.; Beato, P.; Swang, O.; Svelle, S. Kinetics of Zeolite Dealumination: Insights from H-SSZ-13. *ACS Catal.* **2015**, *5*, 7131–7139.
- (42) Henkelman, G.; Jónsson, H. Improved Tangent Estimate in the Nudged Elastic Band Method for Finding Minimum Energy Paths and Saddle Points. *J. Chem. Phys.* **2000**, *113*, 9978–9985.
- (43) Henkelman, G.; Jónsson, H. A Dimer Method for Finding Saddle Points on High Dimensional Potential Surfaces Using Only First Derivatives. *J. Chem. Phys.* **1999**, *111*, 7010–7022.
- (44) De Moor, B. A.; Reyniers, M.-F.; Marin, G. B. Physisorption and Chemisorption of Alkanes and Alkenes in H-FAU: A Combined Ab Initio–statistical Thermodynamics Study. *Phys. Chem. Chem. Phys.* **2009**, *11*, 2939–2958.
- (45) John, M.; Alexopoulos, K.; Reyniers, M.-F.; Marin, G. B. Reaction Path Analysis for 1-Butanol Dehydration in H-ZSM-5 Zeolite: Ab Initio and Microkinetic Modeling. *J. Catal.* **2015**, *330*, 28–45.
- (46) Ghysels, A.; Verstraelen, T.; Hemelsoet, K.; Waroquier, M.; Van Speybroeck, V. TAMkin: A Versatile Package for Vibrational Analysis and Chemical Kinetics. *J. Chem. Inf. Model.* **2010**, *50*, 1736–1750.
- (47) Olson, D.; Haag, W.; Borghard, W. Use of Water as a Probe of Zeolitic Properties: Interaction of Water with HZSM-5. *Microporous Mesoporous Mater.* **2000**, *35–36*, 435–446.
- (48) Jungstittiwong, S.; Limtrakul, J.; Truong, N. T. Theoretical Study of Modes of Adsorption of Water Dimer on H-ZSM-5 and H-Faujasite Zeolites. *J. Phys. Chem. B* **2005**, *109*, 13342–13351.
- (49) Ding, W.; Klumpp, M.; Li, H.; Schygulla, U.; Pfeifer, P.; Schwieger, W.; Haas-Santo, K.; Dittmeyer, R. Investigation of High-Temperature and High-Pressure Gas Adsorption in Zeolite H-ZSM-5 via the Langmuir Crystal Microbalance: CO<sub>2</sub>, H<sub>2</sub>O, Methanol, and Dimethyl Ether. *J. Phys. Chem. C* **2015**, *119*, 23478–23485.
- (50) Kondo, J.; Iizuka, M.; Domen, K.; Wakabayashi, F. IR Study of H<sub>2</sub>O Adsorbed on H-ZSM-5. *Langmuir* **1997**, *13*, 747–750.
- (51) Jentys, A.; Warecka, G.; Derewinski, M.; Lercher, J. A. Adsorption of Water on ZSM 5 Zeolites. *J. Phys. Chem.* **1989**, *93*, 4837–4843.
- (52) Sokol, A. A.; Catlow, C. R. A.; Garcés, J. M.; Kuperman, A. Computational Investigation into the Origins of Lewis Acidity in Zeolites. *Adv. Mater.* **2000**, *12*, 1801–1805.
- (53) Sokol, A. A. S.; Catlow, C. R. A.; Garcés, J. M. G.; Kuperman, A. Local States in Microporous Silica and Aluminum Silicate Materials. 1. Modeling Structure, Formation, and Transformation of Common Hydrogen Containing Defects. *J. Phys. Chem. B* **2002**, *106*, 6163–6177.
- (54) Bolis, V.; Busco, C.; Ugliengo, P. Thermodynamic Study of Water Adsorption in High-Silica Zeolites. *J. Phys. Chem. B* **2006**, *110*, 14849–14859.
- (55) Ong, L. H.; Dömök, M.; Olindo, R.; van Veen, A. C.; Lercher, J. A. Dealumination of HZSM-5 via Steam-Treatment. *Microporous Mesoporous Mater.* **2012**, *164*, 9–20.
- (56) Gola, A.; Rebours, B.; Milazzo, E.; Lynch, J.; Benazzi, E.; Lacombe, S.; Delevoye, L.; Fernandez, C. Effect of Leaching Agent in the Dealumination of Stabilized Y Zeolites. *Microporous Mesoporous Mater.* **2000**, *40*, 73–83.
- (57) Fjermestad, T.; Svelle, S.; Swang, O. Mechanism of Si Island Formation in SAPO-34. *J. Phys. Chem. C* **2015**, *119*, 2086–2095.
- (58) Agostini, G.; Lamberti, C.; Palin, L.; Milanesio, M.; Danilina, N.; Xu, B.; Janousch, M.; Van Bokhoven, J. A. In Situ XAS and XRPD Parametric Rietveld Refinement to Understand Dealumination of Y Zeolite Catalyst. *J. Am. Chem. Soc.* **2010**, *132*, 667–678.